UNIVERSIDADE ESTADUAL DE CAMPINAS

Instituto de Física Gleb Wataghin

MATHEUS MELO SANTOS VELLOSO

OTIMIZAÇÃO ONLINE DA ABERTURA DINÂMICA DO SIRIUS

ONLINE OPTIMIZATION OF SIRIUS DYNAMIC APERTURE

CAMPINAS

2023

MATHEUS MELO SANTOS VELLOSO

ONLINE OPTIMIZATION OF SIRIUS DYNAMIC APERTURE

OTIMIZAÇÃO ONLINE DA ABERTURA DINÂMICA DO SIRIUS

Dissertação apresentada ao Instituto de Física Gleb Wataghin da Universidade Estadual de Campinas como parte dos requisitos exigidos para a obtenção do título de MESTRE EM FÍSICA, na Área de FÍSICA.

Thesis presented to the Gleb Wataghin Institute of Physics of the University of Campinas in partial fulfillment of the requirements for the degree of MASTER IN PHYSICS, in the area of PHYSICS.

Orientadora: LIU LIN

Coorientador: ANTONIO RUBENS DE CASTRO BRITTO

ESTE TRABALHO CORRESPONDE À VERSÃO FINAL DA TESE DEFENDIDA PELO ALUNO MATHEUS MELO SANTOS VELLOSO E ORIENTADA PELO PROF. DR. LIU LIN.

CAMPINAS

2023

FICHA CATALOGRÁFICA

FOLHA DA APROVAÇÃO

Acknowledgements

Lorem ipsum dolor sit amet, consectetuer adipiscing elit. Ut purus elit, vestibulum ut, placerat ac, adipiscing vitae, felis. Curabitur dictum gravida mauris. Nam arcu libero, nonummy eget, consectetuer id, vulputate a, magna. Donec vehicula augue eu neque. Pellentesque habitant morbi tristique senectus et netus et malesuada fames ac turpis egestas. Mauris ut leo. Cras viverra metus rhoncus sem. Nulla et lectus vestibulum urna fringilla ultrices. Phasellus eu tellus sit amet tortor gravida placerat. Integer sapien est, iaculis in, pretium quis, viverra ac, nunc. Praesent eget sem vel leo ultrices bibendum. Aenean faucibus. Morbi dolor nulla, malesuada eu, pulvinar at, mollis ac, nulla. Curabitur auctor semper nulla. Donec varius orci eget risus. Duis nibh mi, congue eu, accumsan eleifend, sagittis quis, diam. Duis eget orci sit amet orci dignissim rutrum.

Resumo

Lorem ipsum dolor sit amet, consectetuer adipiscing elit. Ut purus elit, vestibulum ut, placerat ac, adipiscing vitae, felis. Curabitur dictum gravida mauris. Nam arcu libero, nonummy eget, consectetuer id, vulputate a, magna. Donec vehicula augue eu neque. Pellentesque habitant morbi tristique senectus et netus et malesuada fames ac turpis egestas. Mauris ut leo. Cras viverra metus rhoncus sem. Nulla et lectus vestibulum urna fringilla ultrices. Phasellus eu tellus sit amet tortor gravida placerat. Integer sapien est, iaculis in, pretium quis, viverra ac, nunc. Praesent eget sem vel leo ultrices bibendum. Aenean faucibus. Morbi dolor nulla, malesuada eu, pulvinar at, mollis ac, nulla. Curabitur auctor semper nulla. Donec varius orci eget risus. Duis nibh mi, congue eu, accumsan eleifend, sagittis quis, diam. Duis eget orci sit amet orci dignissim rutrum.

Abstract

Beam accumulation into the SIRIUS storage ring occurs in the off-axis scheme, for which the efficiency depends on a sufficiently large dynamic aperture (DA) - the region comprising stable transverse oscillations. In the design phase, SIRIUS DA was numerically optimized in the accelerator model using various techniques and during commissioning the optimized lattice was implemented in the machine. Recent measurements indicate that SIRIUS DA, although sufficiently large for an injection efficiency of around 85%, can be yet increased upon fine-tuning of sextupole magnets strengths, which govern the beam nonlinear dynamics and determine the DA. In this master's project, the student will carry out online optimization experiments to tune the ring nonlinear lattice and improve the DA and injection efficiency into the storage ring.

List of Figures

List of Tables

Contents

CHAPTER 1

Introduction

This dissertation concerns the work performed on the SIRIUS storage ring sextupole mangets with the objective to optimize the ring's Dynamic Aperture (DA) and injection efficiency. The text is organized as follows:

- The present chapter introduces synchrotron light sources, the SIRIUS project, the main components and subsystems found in electron storage rings and the problem trackled during the execution of the masters project;

- Chapter 2 introduces the theoretical and scientific background on the dynamics of particles in accelerators;

- Chapter 3 introduces and justifies online optimization in accelerators and the Robust Conjugate Direction Search (RCDS) algorithm;

- Chapter 4 describes the experimental methods and setup for the online optmization experiments and the results achieved;

- Chapter 5 concludes this dissertation presenting the final remarks.

1.1   Storage ring-based synchrotron light sources

Synchrotron radiation (SR) is the electromagnetic radiation emitted by charged relativistic particles when accelerated perpendicularly to their motion. The phenomenon was theoretically predicted in the early 1900s when Liénard and Wiechert calculated the retarded potentials for point particles. The first experimental observation occurred at General Electric's synchrotron accelerator, justifying the adoption of the term "synchrotron" in its name [1].

Synchrotron light is extermely colimated and has a broad spectral distribution, covering from infrared to hard X-rays. These properties make synchrotron light ideal for imaging experiments in crystallography and spectroscopy in a wide variaty of scientific disciplines.

Modern synchrotron light sources primarily rely on two particle acceleration technologies: free-electron lasers and electron storage rings. Here, we focus on storage

ring-based synchrotron light source facilities. In these facilities, ultra-relativistic electron beams are stored for extended periods within a chamber in ultra-high vacuum to produce synchrotron light. The beams are maintained in stable orbits by the fields of an array of magnets–the lattice–which provide both bending, focusing and trajectory-correction fields. The beam is also periodically influenced by radiofrequency cavities, which replenish the energy radiated away in the form of light.

The main figure of merit for the quality of a SR source is the *brightness* [2], defined as the photon flux in six-dimensional phase space [3]:

$$B(\omega) = \frac{1}{\Delta\omega/\omega} \frac{F(\omega)}{\Sigma_x(\omega)\Sigma_y(\omega)}, \tag{1.1}$$

where $F(\omega)$ is the photon flux at energy $E = \hbar\omega$, Σ_u is the photon beam volume in the the $u = x, y$ phase space, and $\Delta\omega/\omega$ is the frquency bandwith, which is typically about 0.1%. The photon phase space volume depends on the convolution of the electron beam distribution with the distribution of the photons emmited by a single electron. The latter depends on the photon energy and the emission process, while the former is related to the average phase space volume of the electron beam: the *emmitance*, which depends on the magnetic lattice and has units of the transverse phase space areas (length times angle). Increasing brightness depends on maximizing the photon flux, reducing the electron beam emittances and optimizing the matching between photon and electron beams for maximizing their distributions convolution [1].

Synchrotron light sources can be classified based on their brightness/emmitances. In the early 1960s, the community interested in synchrotron radiation (SR) for imaging experiments obtained SR parasitically from high-energy and nuclear physics machines such as DESY and DORIS in Germany and ADA in Italy [4], marking the era of first-generation synchrotron light sources [5]. The second-generation machines emerged in the 1980s and consisted on machines designed exclusively for SR production, such as BESSY, DORIS II and III, ELSA in Germany, SUPERACO in France, MAX I in Sweden [4] and UVX in Brazil.

The 1990s saw a growing demand for higher brightness, leading to the development of third-generation machines [5]. These machines introduced insertion devices such as wigglers and undulators, significantly enhancing brightness by increasing radiative damping. Additionally, these devices allowed precise control over radiation energy and polarization. Typical emmitance for third-generation machines is of the order of units to tens of nm rad. Most of currently operating machines pertain to the third-generation, such as ALBA in Spain, ESRF and SOLEIL in France, Diamond in the United Kindom and ELETTRA, in Italy [4].

The era of the fourth-generation of storage rings (4GSR) commenced with the commissioning of the MAX-IV machine in Lund, Sweden, in 2015 [3,5]. Fourth-generation

machines achieved a notable reduction in emittance, reaching sub-nm rad values thanks to recent technological advancements in computer simulations, vaccum technology, machining and mechanical alignment [3, 5]. Following MAX-IV, an upgrade of the ESRF facility, the ESRF-EBS, and the launch of SIRIUS in Campinas marked significant milestones for the fourth-generation. Today, several 4GSR projects are being planned, designed and constructed.

1.2 The SIRIUS project

SIRIUS is a 4GSR synchrotron light source. It was designed, built, and is operated by the Brazilian Synchrotron Light Laboratory (LNLS), on the campus of the Center of Research in Energy and Materials (CNPEM), in Campinas, Brazil. The storage ring operating energy is 3 GeV, and the ring has 518 m in circumference. The natural emmitance of the lattice is 250 pm rad and it is expected to reach 150 pm rad with the installation of its definitive insertion devices [6][1].

SIRIUS succeeded the first synchrotron light source in Brazil, the UVX machine, which opened to users in 1997 and served the community until its shutdown, in the beginning of SIRIUS commissioning, in August 2019[2] [6]. The project started in 2009, initially planned and designed as a third-generation machine. By 2012, it evolved into the project of a fourth-generation machine [6]. Cunstruction was finished in 2018, when the LINAC and Booster commissioning started. In november 2019 the first beam was stored in the storage ring.

> Check these statemets. Get more info about main milestones

SIRIUS finished its Phase-0 commissioning in 2022 and since March 2023 is receiving its first external users. At the time of this writing, it has 6 operating beamlines, 4 beamlines in commissioning and 4 under construction and installation. It is currently operating for user's beam with a 100 mA current, with frequent beam injections throughout the day, a scheme known as "top-up" mode. SIRIUS is expected to achieve 350 mA current when the system of two superconducting radiofrequency cavities is installed [7, 8].

> more info on the phases. which phase are we in?

Presently, SIRIUS stands as the most complex scientific infrastructure ever consturcted in Brazil, with the ambitious goal of positioning the country at the forefront of global leadership in synchrotron light sources. This state-of-the-art synchrotron was meticulously designed to shine as the brightest in its energy category, and has the capacity

---

[1]SIRIUS is currently operating with provisional insertion devices for providing light to the first users and allowing scientific commissioning of the beamlines

[2]The UVX project led to the creation of LNLS, which marked a new model for scientific research in Brazil, based on social organizations under contracts with the Ministry of Science Technology and Innovations. LNLS paved the way for national labs (NL), including labs on biosciences (LNBio), nanotechnology (LNNano), and bio-renewables (LNBR), which are also located at the CNPEM campus.

Figure 1.1: Schematic view of the SIRIUS installations. 1) Linear accelerator (LINAC); 2) Concrete tunnel housing the booster accelerator and the storage ring; 3) storage ring; 4) beamlines. From LNLS website.

to host up to 40 beamlines. As of the time of this writing, SIRIUS holds the distinction of being the sole fourth-generation synchrotron radiation source in the southern hemisphere and one of merely three 4GSRs in operation across the globe (still true?).

1.3   Subsystems and components of a storage ring-based light source facility

Typical systems comprising a storage ring synchrotron light source facility include:

- an injection system: including the electrons source, beam transport lines, the linear accelerator and the booster circular accelerator. At SIRIUS, the linear accelerator provides the booster ring with a 150 MeV beam. The booster further ramps the beam energy up to 3 GeV, which is the storage ring operation energy;

- storage ring: where ultra-relativistic electrons are kept stable for hours within the vaccum-chamber, oscillating about a closed orbit for the production of synchrotron light;

- beamlines which steer the photon beams towards the experimental cabins where samples are placed for the experiments based on light-matter interaction, such as spectroscopy, crystallography, tomography and others.

A schematic view of the SIRIUS building is shown in Fig. 1.1.

In a synchrotron storage ring, ultra-relativistic electron beams are stored in proximity to a reference design orbit. This orbit is determined by the strengths of the

deflection magnets, the dipoles, and the operation energy of the beams. A pure dipole provides an uniform and homogeneous magnetic field perpendicular to the floor. To define a closed orbit, the overall bending angle provided by the dipoles along the entire ring must equal 2π radians. The field profile of a dipole magnet is depicted in the left side sketch of Fig. 1.2. Imagining a beam directed inward the screen, the trajectory will be bent to the right.

To maintain electrons in close proximity to the reference orbit, focusing is achieved through gradient fields, primarily generated by quadrupole magnets at SIRIUS. The strength of such fields increase linearly with deviations from the closed orbit, which lies in the magnet's center. Gradient fields effectively act as spring forces. The mangets poles and the field profile of a quadrupole magnet are depicted in the center sketch of Fig. 1.2.

Focusing and deflection are energy-dependent, which means small deviations from the nominal operating energy can result in differential focusing. Drawing an analogy from geometric optics, the beam's focusing behavior at the "lens" (quadrupoles) depends on its "color" (energy). To correct for these chromatic aberrations, the use of "glasses" becomes necessary. In the context of accelerators, sextupole fields serve as these corrective lenses. They introduce geometric aberrations to counteract the chromatic ones, resulting in approximately uniform, energy-independent focusing. The mangets poles and the field profile of a sextupole magnet are depicted in the right sketch of Fig. 1.2.
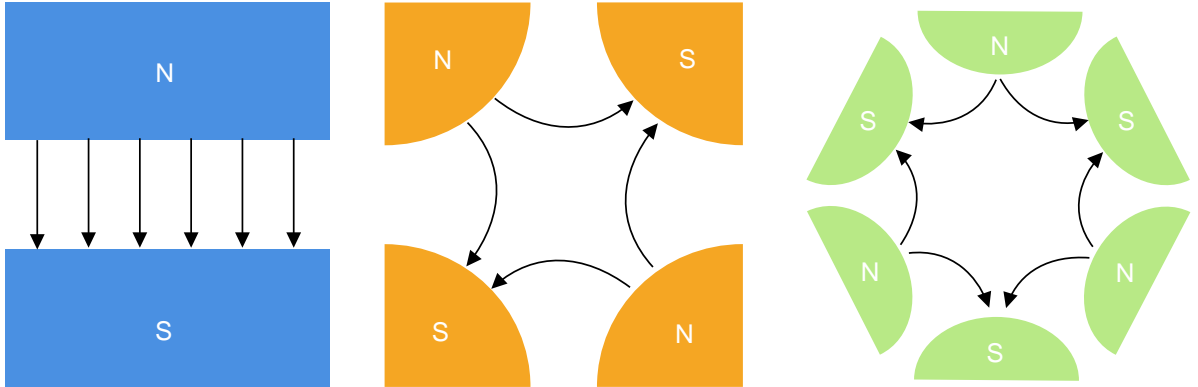
Figure 1.2: Schematic representation of the magnets comprising SIRIUS lattice and their fields profile. From left to right: dipole magnet, quadrupole magnet and sextupole magnet.

Besides dipoles, quadrupoles and sextupoles, additional dipole actuators magnets for orbit/trajectory correction and pulsed magnets for beam extraction and injection can also be found in SIRIUS.

The beam is also periodically subject to longitudinal time-dependent electromagnetic radiofrequency fields which do work on the beam to replenish its energy. The

goal is to compensate for the energy carried away in the form of synchrotron light.

1.4   The problem addresed in this work

The pursuit of low emittances and high brightness has driven the accelerator community toward the fourth-generation of storage rings. Achieving such low emittances was possible because of series of technological advances which enabled the use of the multi-bend achromat (MBA) lattice [3, 5]. MBA lattices require intense gradient fields provided by quadrupole magnets, which, in turn, demands the presence of strong sextupolar fields to compensate for chromatic effects. Since sextupoles provide nonlinear fields, the dynamics in fourth-generation storage rings has become increasingly nonlinear [5].

A quasi-periodic nonlinear dynamics, when subjected to even the slightest perturbations—such as small field errors stemming from rotation, alignment, or fields excitation errors—can potentially become unstable at large oscillation amplitudes. These instabilities impose constraints on the maximum transverse oscillation amplitudes that the machine can accommodate. The specific amplitude below which motion is stable is referred to as the Dynamic Aperture (DA) of the ring. Exceeding the DA results in irregular and often chaotic motion and beam loss.

Under normal operating conditions, the equilibrium beam size and typical oscillation amplitudes are considerably smaller than the DA, and the dynamics can be well studied and analyzed using a linear approximation theory, without worrying about the DA. However, there are specific scenarios where the DA becomes crucial for the operation, notably during the injection process.

During injection into the storage ring for beam accumulation, the beam is extracted from the booster accelerator and guided toward the storage ring through a transport line. As soon as it enters the ring, the beam is deflected by the field of a pulsed nonlinear magnet, which makes the beam almost parallel to the storage ring tangent direction, albeit with a horizontal offset of approximately $x = -8$ mm [9]. If the DA is smaller than this initial amplitude, it imposes limitations on the injection efficiency.

The placement, symmetry and strength of sextupoles magnets–the nonlinear lattice– were determined through a multi-objective optimization process, primarily focused on improving the simulated DA and beam lifetime of the machine's computer model [10, 11]. This optimization work considered the average performance of the lattice configurations while accounting for various magnet errors that simulate the expected errors in the actual machine [10]. Several models, with several errors distribution among the magnets were generated, and the DA and lifetime for a given lattice configuration was calculated by simulating the electron beams motion for several turns (tracking simulations). The final figure of merit for a lattice consisted on the average DA and lifetime it provided to the ensemble of machines. The best-performing machine lattice found during this process

was adopted as the nominal lattice which was subsequently implemented during the commissioning phase of the machine.

The operating machine consists on a practical realization of a specific error configuration, which defines the physically realized magnetic lattice and the dynamics overall performance. The best-performing lattice on average is not necessarily the optimum lattice for this errors realization.

Assuming the realized lattice closely approximates the optimum setup, i.e. that errors are small, it is reasonable to assume that making minor tweaks and adjustments to the strengths of the sextupoles can adapt the lattice to match the actual distribution of errors in the physical system. This fine-tuning process can result in improved nonlinear dynamics performance, expanding the DA, and ultimately enhancing both injection efficiency and its stability. This process has already been demostraded in other machines. It has proven to be a succesfull approach and became knonw as *Online optimization*. Online optimization of the machine nonlinear dynamics consists on employing computer-automated search strategies to systematically explore various sextupole configurations with the goal of identifying the one that yields the largest DA while not interfering in other machine parameters, such as chromaticity and beam lifetime.

The key ingredient in online optimization is the choice of a robust optmization algorithm based on direct or indirect search in the parameter space. The most widely used is the Robust Conjugate Direction Search (RCDS) algorithm, which is based on a noise robust one-dimensional optimizer along with a clever strategy, known as Powell's method, for choosing directions in the search space.

In agreement with the experience in other facilities, it is shown in this dissertation that online optimization using RCDS can succesfully improve the dynamics performance and lead to DA and injection efficiency improvements. Prior to the optimization work, the DA was measured to be X, which rendered an average of X% injection efficiency. The main difficulty was the typycal fluctuations in the effciency .

This demonstration is valuable because it is a benchmark test for the method applied to fourth-generation rings with such a large search space. SIRIUS has 21 sextupole families. Online optimization has been performed also at XXXX, which have way less search parameters.

check: online optimization has been carried out on MAXIV - how many families they have? Any other 4GSR? ERSF?

Assuming the realized lattice closely approximates the optimum setup, i.e. that errors are small, it is reasonable to assume that making minor tweaks and adjustments to the strengths of the sextupoles can adapt the lattice to match the actual distribution of errors in the physical system. This fine-tuning process can result in improved nonlinear dynamics performance, expanding the Dynamic Aperture (DA), and ultimately enhancing injection efficiency and its stability.

Online optimization consists on employing computer-automated search strategies to systematically explore various sextupole configurations with the goal of identifying the one that yields the largest dynamic aperture while not interfering in other machine parameters. We specilize to online optimization using the Robust Conjugate Direction Search algorithm, which has been broadly applied to optimization in accelerators.

It is shown in this dissertation that this optimization process can succesfully improve the dynamics performance. Prior to the optimization work, the Dynamic Aperture was measured to be , which rendered an average of injection efficiency. The main difficulty was the typycal fluctuations in the effciency .

Besides improving the injection efficiency in ordinary operation conditions, it is also interesting to do so in different machine *working points*, with different *tunes*. As chapter 2 shows, if one fixes his or her attention to a specific point of the ring, and measure the beam position in horizontal and vertical planes for consecutive turns, one realizes the motion is a sampled sinusoid. The tunes ν_x and ν_y are the fundamental frequencies of such harmonic motion. They are important operation parameters since they affect over the response of the system in the presence of pertrubations. Tunes close to integer numbers make the dynamics particularly sensitive to perturbations. SIRIUS nominal tunes fractional parts are quite low, and increasing them push the tunes away from integers, reducing the *orbit amplification factors* when the orbit is disturbed. Increasing the tunes can be achieved by actuating wiht the quadrupoles, but doing so brings the machine to a different optics, in which the DA can, and indeed is as we shall see, smaller than the expected value. In different working points, the online optimization is essential to achieve a good DA rendering acceptable injection efficiencies for operation.

In this work we show how we have succesfully optimized the dynamic aperture and injection efficiency in the nominal tunes and in different machine working points. At the time of this writing, the machine is operating with the optics found during one of the experiments carried out during the execution of this project. We show how the increased tunes led to unprecedent orbit stability and how online optimization made possible to achieve high injection efficiencies, which allowed for the operation with these tunes.

CHAPTER 2

Theoretical Background

This chapter provides the bare minimum theoretical knowledge on electron storage ring physics and particles dynamics needed to state to the reader the optimization problem and the constraints which are involved. A qualitative description of the physics of electron storage rings is presented, followed by a more detailed and more quantitative treatment of single particle dynamics in storage rings.

2.1 The physics of electron storage rings

As mentioned previously, a storage ring is designed to confine bunches of electrons and steer them along a reference closed orbit. The orbit is defined by the bending magnets, the dipoles. The trajectories consist on oscillations about the closed orbit, and focusing of such oscillations toward the closed orbit is provided by gradient fields, mostly coming from quadrupole magnets. Additionally, to correct chromatic aberrations in the beam's motion, i.e. a dependence of focusing with the beam's energy, and guarantee correct focusing despite energy deviations from the nominal value, sextupolar magnetic fields are also introduced, providing fields depending qudratically on the deviations from the nominal orbit. These fields introduce strong nonlinearities in the dynamics.

When having its trajectory bent at the dipoles and insertion devices[1], the beam loses energy in the form of synchrotron radiation. To mantain the beam stored, the energy lost must be replenished. To this aim, radio-frequency (RF) cavities are placed along the ring to provide oscilating electric fields parallel to the longitudinal direction. The work done in the beam by the fields restore its energy.

The radiated photons are emitted in a narrow cone with angular aperture of $1/\gamma$, γ being the relativistic Lorentz factor (~ 6000 at SIRIUS storage ring). The photons carry away a fraction of the beam's energy and momentum in both the longitudinal and transverse directions. When passing through RF cavities, only momentum in the longitudinal direction is replenished. Radiating photons thus leads to an overall damping of transverse amplitudes.

---

[1]Insertion devices (IDs) consist on arrays of magnetic blocks arranged to provide additional deflection of the beam's trajectory for the production of synchrotron radiation. IDs allow for fine-tuning of the fields and as consequence of the characteristics of the emitted readiation, such as the energy and polarization.

On the other hand, the quantum nature of the emitted radiation leads to the excitation of transverse oscillations, which is known as quantum excitation. When a photon carries away energy, it depletes the electrons energy by the same amount. It thus changes the reference orbit of the electron in certain regions of the ring (dispersive regions), inducing oscillations. Eventually, equillibrium between radiative damping and quantum excitation is achieved, leading the rms values of each electron's amplitudes to reach a stationary regime.

> include the case of nondispersive and vertical amplitudes damping

Each one of the beam's degrees of freedom defines an acceptance: limits which if exceeded can lead to instabilities and eventually beam losses. The most obvious acceptance is the transverse acceptance: the beam motion is bounded by a vacuum chamber and collisions with the chamber's physical apperture leads to losses. Additionally, the beam also has an energy acceptance: a tolerance for energy deviations from the nominal value that when exceeded can lead to a suboptimal energetic balance, deviations from the nominal orbit and eventually collisions with the vacuum chamber.

The beam is also subject to elastic and inelastic collisions with residual gas molecules within the chamber and also the collisions between electrons within the same bunch, besides other kinds of interactions with wake-fields from other bunches. The overall beam loss rate defines the characteristic time scale at which a given electron current survives in the ring. This is the beam lifetime and determines the rate at which injections into the storage ring are required.

Because of the nonlinearities introduced by the sextupole magnets, the transverse acceptances can be limited not by the physical aperture but rather by the amplitudes above which motion is irregular, unstable and unbounded. As already mentioned before, this limiting amplitude is known as the dynamic aperture (DA), a term that can be used to refer to amplitudes in the transverse space x, y or to the phase space coordinates x, p_x and y, p_y.

Despite the complicated physics of a fully-coupled dynamics involving the transverse and the energy oscillations and also the damping and the excitation of amplitudes, collective effects and instabilities, for the purpose of this dissertation, it is sufficient to model the motion of a single electron, negletcting radiation losses and any other collective interactions.

In this picture, the electron travels along the ring at the speed of light and executes transverse oscillations in two orthogonal planes. The dynamics takes place in a 4-dimensional phase space which is the dynamics of two independent quasi-periodic oscillators. These simplfications are justified for our immediate purposes because:

- radiation losses/gains and energy oscillations are only significant over a time scale of a couple of turns. Over this period, tens of transverse oscilations take place

- the linear, uncoupled dynamics this modeling renders serves as a building block upon which ellaborate modeling can be carried out, incoporating coupling, nonlinearities and perturbations

- why is ok to ignore collective effects and instabilities?

Next, the single-particle dynamics is presented with the aim of defining quantitavely the dynamic aperture and the characteristics of the dynamics in electron strorage rings. Throghout the modelling, optical functions and parameter for the SIRIUS storage rings are also presented.

2.2 Motion of charged particles in magnetic fields

An electron of charge e and momentum p follows a circular orbit of radius ρ when interacting with an uniform and time-independent magnetic field of magnitude B, pointing along the perpendicular to the ortbit plane. In such conditions, Lorentz force law predicts that

$$R(p) \equiv B\rho = \frac{p}{e}. \tag{2.1}$$

Consider now an electron traveling along a curve parametrized by the arclength s with respect to an arbitrary reference point. The interaction with fields $B_x(x, y, s)$ and $B_y(x, y, s)$, both perpendicular to the electron's motion, results in deflections of the trajectory. The deflection angles are given by

$$
\begin{aligned}
\mathrm{d}\theta_x &= \frac{\mathrm{d}s}{\rho_x(s)} = \frac{e}{p} B_y(x, y, s)\mathrm{d}s = \frac{1}{R(p)} B_y(x, y, s)\mathrm{d}s, \\
\mathrm{d}\theta_y &= \frac{\mathrm{d}s}{\rho_y(s)} = \frac{e}{p} B_x(x, y, s)\mathrm{d}s = \frac{1}{R(p)} B_y(x, y, s)\mathrm{d}s.
\end{aligned}
\tag{2.2}
$$

Where (2.1) has been used to replace the p/e ratio by the *magnetic rigity* $R(p)$, which is defined as the product of the uniform field strength needed for a beam with momentum p and charge e to perform circular orbit with radius ρ. The rigidity depends solely on the electron's momentum/energy and gives the appropriate normalization to evaluate the instantaneous angular deflections in the electron's trajectory caused by magnetic fields.
Add deflection figures

2.3 Storage rings

draw my onw figure

Figure 2.1 sketches the typical design of a storage ring. For the porpose of storing a beam of electrons in closed orbits, magnetic fields defining a closed orbit are
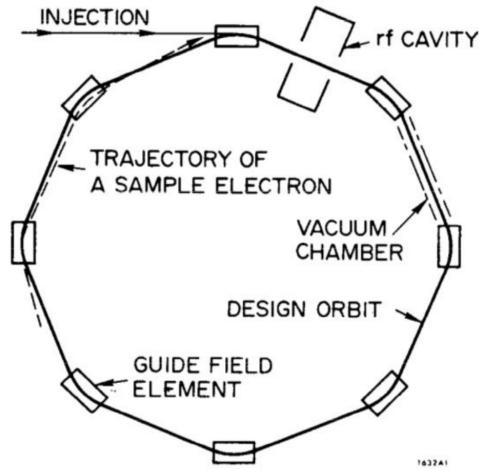
Figure 2.1: Storage ring typycal configuration. From [**?**]

necessary. The angular deflections should add up to 2π, and the specification of the beam's operating energy determines the integrated field required for causing the closed orbit deflections.

For providing stability, focusing towards the reference closed orbit is also needed, and can be attained with the introduction of gradient fields whose strengths depend linearly on the tranverse excursions from the reference orbit. Such fields are provided mainly by quadrupole magnets, which are physically realized by specifying magnetic poles with the shape of truncated hyperbolas.

Sextupole mangets are also usually included in the design of storage rings. The fields they produce is quadratic with transverse displacement and are needed for correction of chromatic errors in the dynamics.

add magnets and field profile figures

2.4 The coordinate system

A convinient coordinate frame to decribe the dynamics in storge rings can be constructed by imagining a reference particle traveling along a curve drawn by the tip of a vector $\mathbf{r}_0$, as Fig. 2.2 shows. The particle travels a distance s along the ring, which can be used to parametrize the motion. The triad of direction vectors consists of a vector $\hat{\mathbf{s}}$, tangent to the trajectory, a vector $\hat{\mathbf{x}}$ normal to it, pointing in the direction at which $\hat{\mathbf{s}}$ changes and a vector $\hat{\mathbf{y}} = \hat{\mathbf{x}} \times \hat{\mathbf{s}}$, bi-normal to the trajectory. This construction leads to a Frenet-Serret reference frame.

Assuming no curvature in the y plane, i.e. that the accelerator defines a curve whose plane is parallel to the ground, then the unit vectors defining the frame can be
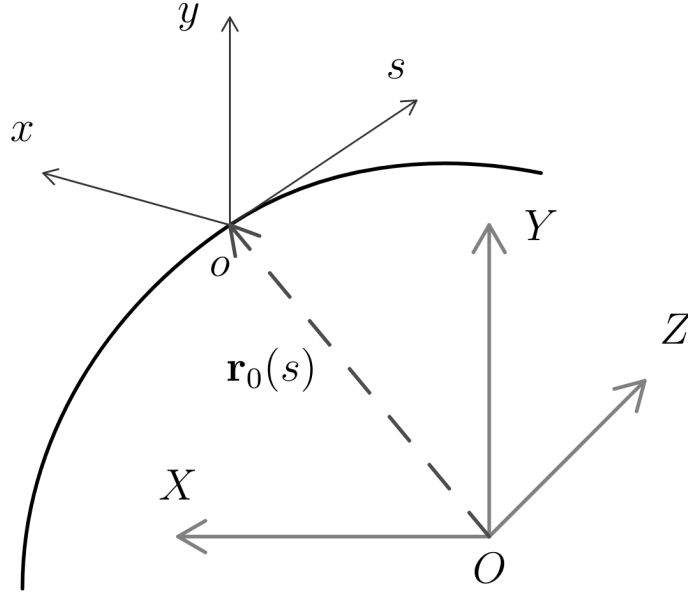
Figure 2.2: The Frenet-Serret coordinate system. From [**?**].

calculated by [**?**]

$$\hat{\mathbf{s}} = \frac{d\mathbf{r}_0}{ds}, \quad \hat{\mathbf{x}} = -\rho\frac{d\hat{\mathbf{s}}}{ds}, \quad \hat{\mathbf{y}} = \hat{\mathbf{x}} \times \hat{\mathbf{s}}, \tag{2.3}$$

where $\rho(s) = \|d\hat{\mathbf{s}}/ds\|^{-1}$ is the local curvature radius[2]. The vectors evolve along s as prescribed by the Frenet-Serret equations:

$$\frac{d\hat{\mathbf{s}}}{ds} = -\frac{1}{\rho(s)}\hat{\mathbf{x}}, \quad \frac{d\hat{\mathbf{x}}}{ds} = \frac{1}{\rho(s)}\hat{\mathbf{s}}, \quad \frac{d\hat{\mathbf{y}}}{ds} = 0, \tag{2.4}$$

The frame thus depends solely on the geometry of the specified path. Since the curvature is defined by the dipolar fields $B_0(s)$ in the y direction, then, eq. (2.2) leads to

$$G(s) \equiv \frac{1}{\rho(s)} = \frac{B_0(s)}{R_0}, \tag{2.5}$$

where R_0 is the rigidity for the beam at the nominal energy.

2.5   Hamiltonian for the relativistic electron

The dynamics of relativistic electrons influenced by electromagnetic fields $(\Phi, \mathbf{A})$ is encapsulated by the Hamiltonian

$$H = \sqrt{m^2c^4 + (\mathbf{P} - q\mathbf{A})^2c^2} + e\Phi,$$

---

[2]For a circular trajectory, $\mathbf{r}_0 = (R\cos(s/R), R\sin(s/R), 0)$, $0 \leq s \leq L$ (check), in the cartesian laboratory frame. $\hat{\mathbf{s}} = (-\sin(s/R), \cos(s/R), 0)$, $d\hat{\mathbf{s}}/ds = -R^{-1}(\cos(s/R), \sin(s/R), 0)$ and $\rho(s) = R$

e being the elementary charge and $\mathbf{P} = \mathbf{p} + e\mathbf{A}$ the canonical momentum. The following steps are followed to obtain equations of motion for electrons in the storage ring:

- A canonical transformation to change coordinates is applied in order to describe the motion in terms of the Frenet-Serret frame variables x, y;

- Instead of time t, the Hamiltonian and the dynamical variables are described as functions of s, the longitudinal position along the ring;

- Geometric quantities are used: canonical momenta are the angles $x' = \mathrm{d}x/\mathrm{d}s$ and $y' = \mathrm{d}y/\mathrm{d}s$ with respect to the nominal orbit;

- Paraxial approximation: transverse momenta are assumed to be way smaller than longitudinal momentum;

All of these steps are shown in detail in textbooks such as Refs. [**?**, **?**, **?**]. Neglecting RF cavities ($\Phi = 0$) and radiation losses, the energy is a constant parameter and the dynamics will consist solely on the transverse degrees of freedom. In this 4-dimensional dynamics, the set of canonical variables are (x, p_x, y, p_y), where

$$\begin{cases} p_x = x'(1 + \delta), \\ p_y = y'(1 + \delta), \end{cases} \tag{2.6}$$

and

$$\delta = \frac{P - P_0}{P_0} \approx \frac{E - E_0}{E_0} \tag{2.7}$$

where the ultra-relativistic approximation $E \approx pc$ was used.

Hamilton's equations for the Hamiltonian in the paraxial approximation lead to the equations of motion for 4D dynamics

$$x'' = -\frac{(1 + Gx)^2}{1 + \delta}\frac{B_y}{R_0} + G(1 + Gx), \quad y'' = \frac{(1 + Gx)^2}{1 + \delta}\frac{B_x}{R_0} \tag{2.8}$$

where $R_0 = p_0/e$ and $G(s)$ defined as in Eq. (2.5).

Fields influencing the beam are those of dipoles, quadrupoles and sextupoles. Their functional forms are

- Horizontal Dipole:

$$B_x = 0, \quad B_y = B_0$$

- Normal quadrupole

$$B_x = B_1 y, \quad B_y = B_1 x$$

- Normal sextupole

$$B_x = B_2 xy, \quad B_y = \frac{1}{2} B_2 (x^2 - y^2)$$

These are the so-called *normal multipole fields*. There also exists *skew multipole fields*, which couple the horizontal and vertical dynamics. We will neglect skew fields and coupling for now.

In the equations of motion, eqs. (2.8), the magnetic rigidity normalizes all the fields. We define the dipolar, quadrupolar and sextupolar functions by

$$G(s) = \frac{B_0(s)}{B\rho}, \quad K(s) = \frac{B_1(s)}{B\rho}, \quad S(s) = \frac{B_2(s)}{B\rho}. \tag{2.9}$$

2.6 Linear Dynamics

Linear equations of motion

Expansion of eqs. (2.8) up to first order in the x, y, δ variables leads to [**?**]

$$x'' + (G^2 + K)x = G\delta, \quad y'' - Ky = 0. \tag{2.10}$$

For on-momentum particles, $\delta = 0$, both equations reduce to Hill's equations

$$u'' + K_u(s)u = 0, \tag{2.11}$$

which are a pair of parametric oscillators for $u = x, y$, with s-dependent focusing functions

$$K_x(s) = G^2(s) + K(s), \quad K_y(s) = -K(s).$$

Motion in the linear approximation thus consists on oscilations around the closed orbit, known as betatron oscilations.

Pseudoharmonic description

The solutions for the equations of betatron motion can be cast in a amplitude-phase (WKB) form

$$u(s) = \sqrt{2\beta_u(s) J_u} \cos(\phi_u(s) + \phi_0), \tag{2.12}$$

where $\beta_u(s)$ must satify the boundary value problem

$$\frac{1}{2}\beta_u'' + \beta_u K_u(s) - \frac{1}{\beta_u}\left(\frac{1}{4}\beta_u'^2 + 1\right) = 0, \quad \begin{cases} \beta_u(0) = \beta_u(L) \\ \beta_u'(0) = \beta_u'(L) \end{cases} \tag{2.13}$$

and the phase advance must be

$$\phi_u(s) = \int_0^s \frac{1}{\beta_u(\sigma)} \mathrm{d}\sigma. \tag{2.14}$$

The betatron functions for the SIRIUS storage ring are shown in Fig. 2.3.
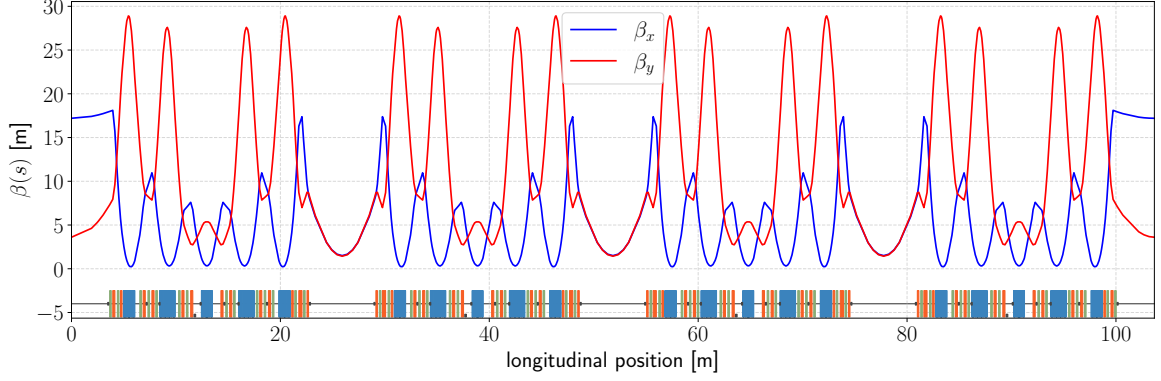
Figure 2.3: Betatron functions for the SIRIUS storage ring. Colored blocks represent the magnets of the accelerator lattice: blue for dipoles, orange for quadrupoles and green for sextupoles. The ring has a 5-fold symmetry, with the lattice and betatron function repeating the same pattern shown above five times up to $s = 518$ m

An important feature of the dynamics is the *tune*: the phase advance per ring revolution

$$\nu_u = \frac{1}{2\pi} \int_s^{s+L} \frac{\mathrm{d}\sigma}{\beta_u(\sigma)} \equiv \frac{1}{2\pi} \oint \frac{\mathrm{d}s}{\beta_u(s)}.$$

The analysis of perturbations and nonlinearities shows that the tunes are a critical variables in determining the beam's response to perturbations. More specifically, the tunes impact over disturbances amplifiction factors, which are greatest when tunes are close to integer numbers.

Turn-by-turn motion

In the u, u' phase space, the quasi-periodic motion traces out ellipses. This can be verified by calculating the derivative

$$u'(s) = -\sqrt{\frac{2J_u}{\beta_u}} \left[\sin(\phi_u(s) + \phi_0) + \frac{1}{2}\beta'_u(s)\cos(\phi_u(s) + \phi_0) \right], \tag{2.15}$$

defining $\alpha_u = \frac{\beta'_u}{2}$ and $\gamma_u = \frac{(1+\alpha_u^2)}{\beta_u}$ and checking that u, u' satify the quadratic form

$$2J_u = \gamma_u u^2 + 2\alpha_u u u' + \beta_u u'^2. \tag{2.16}$$

The ellipse properties are defined by the $\beta(s), \alpha(s)$ and $\gamma(s)$ functions, also known as Courant-Snyder (C-S) parameters or Twiss parameters. Tracking a particle's

transverse position and momenta for several turns at some fixed point along the ring results in the ellipse with shape specified by the C-S parameters. Since the parameters are functions of the position s, then, at each point along the accelerator, the Poincaré Section u, u' displays a different ellipse for each point.

Since the phase advance over a turn is $2\pi\nu + \phi_0$, the phase advance after the j-th turn is $2\pi\nu j + \phi_0$, and thus sampling the transverse motion at a fixed $s = s_0$ position reveals a harmonic displacement

$$u_j(s_0) = \sqrt{2\beta_u(s_0)J_u}\cos(2\pi\nu_u j + \phi_u(s_0)). \tag{2.17}$$
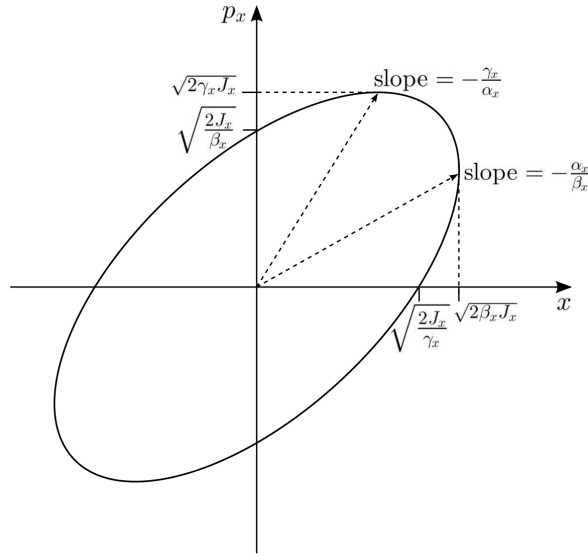
Figure 2.4: Phase space ellipse traced by tur-by-turn (TbT) motion in the (x, p_x) phase space. Optics functions determine the principal axes ratios and the inclination of the ellipse at each longitudinal position along the ring. From [?].

Dispersion

The equation of motion for off-momentum particles in the horizontal plane is the non-homogeneous Hill's equation. The solution consists on the linear combination of the homogeneous solutions in the phase-amplitude form plus the particular solution: $x = x_\beta + x_\delta = x_\beta + \eta(s)\delta$ where $\eta(s)$ is the *dispersion function*, satisfying

$$\eta'' + (G^2 + K)\eta = G, \quad \begin{cases} \eta(0) = \eta(L), \\ \eta'(0) = \eta'(L). \end{cases}$$

The periodicity in the $\eta(s)$ function is required if we want to interpret η as closed orbit per momentum deviation. Thus, off-momentum particles perform betatron oscillations

around a dispersive orbit. The dispersion function for the SIRIUS storage ring is shown in Fig. 2.5
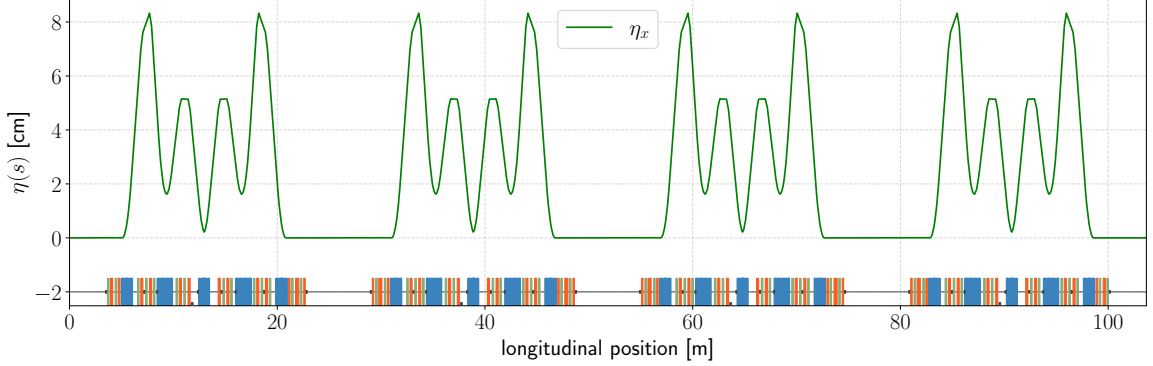
Figure 2.5: Dispersion fucntion for SIRIUS superperiod.

Field Errors

In the presence of additional dipolar and quadrupolar fields ΔG and ΔK, respectively, the orbit and focusing are changed. Assuming these are small perturbations and not strong enough to kill the beam, we can evluate the disturbances to the unperturbed dynamics. The closed orbit distortion due to a single dipole error ΔG reads

$$x_{\mathrm{co}}(s) = \frac{\sqrt{\beta(s)\beta_0}}{2\sin\pi\nu}\Delta G\cos(|\phi(s)-\phi_0|-\pi\nu). \tag{2.18}$$

For a distribution $\Delta G(s)$ of dipolar perturbations along the ring, we sum over the contributions, and obtain the total disturbance

$$x_{\mathrm{co}}(s) = \frac{\sqrt{\beta(s)}}{2\sin\pi\nu}\int_s^{s+L}\Delta G(\sigma)\sqrt{\beta(\sigma)}\cos(\pi\nu+\phi(s)-\phi(\sigma))\mathrm{d}\sigma. \tag{2.19}$$

As for gradient errors, focusing is changed, which leads to changes in the beta function and phase advance. The tune-shift as a consequence of a gradient error present "during" a small extent Δs along the ring is

$$\Delta\nu \approx \frac{1}{4\pi}\beta_0\Delta K\Delta s. \tag{2.20}$$

Again, for a distribution of errors we sum over the ring:

$$\Delta\nu \approx \frac{1}{4\pi}\oint\beta(s)\Delta K(s)\mathrm{d}s. \tag{2.21}$$

Is also possible to show tha the the relative beta-function error, known as beta-beating,

reads

$$\frac{\Delta\beta(s)}{\beta(s)} = -\frac{1}{2\sin(2\pi\nu_0)} \int_s^{s+L} \Delta K(\sigma)\cos(2\phi(\sigma) - 2\phi(s) - \phi_0)\mathrm{d}\sigma. \tag{2.22}$$

Chromaticity

Energy deviations affect not only the closed orbit by means of the dispersion effect. A more/less energetic beam has higer/lower rigidity and thus is focused differently when passes through quadrupoles.

Expanding the equations of motion, (2.8), for off-energy particles up to the order of terms $u\delta$ ($u = x, y$) gives the additional higher-order gradient terms

$$\Delta K_x = -(K_1 + 2G^2)\delta \approx K_x\delta \tag{2.23}$$

$$\Delta K_y = K_1\delta = -K_y\delta \tag{2.24}$$

This means there exists an energy-dependent tune-shift effect, which, using eq. (2.21), reads

$$\Delta\nu_i \approx -\frac{1}{4\pi} \oint \beta K_i\delta\,\mathrm{d}s\,, \tag{2.25}$$

for the $i = x, y$ planes.

We can define the *linear chromaticity* in the $i = x, y$ direction as energy error-induced tune-shift $\Delta\nu_i$ per energy deviation δ

$$\xi_i = \frac{\mathrm{d}\nu_i}{\mathrm{d}\delta}. \tag{2.26}$$

This uncorrected chromaticity is also called natural chromaticity. Using expression (2.25) for the tune-shift, the natural chromaticity reads

$$\xi_{i,\mathrm{nat}} \approx -\frac{1}{4\pi} \oint K_i\beta_i\,\mathrm{d}s\,. \tag{2.27}$$

To correct this chromatic effect, we need to introduce sextupolar fields in the lattice, specifically in the dispersive regions. In such regions, off-energy particles should have a deviation from the design closed orbit. Their position reads $x(s) = x_\beta(s) + \eta(s)\delta$, where $x_\beta(s)$ consists on the betatron oscillations. Since sextupolar fields are of the form

$$B_x = B_2 xy, \quad B_y = \frac{B_2}{2}(x^2 - y^2),$$

then, the off-momentum particles "see" the fields

$$B_x = B_2(x_\beta y + \eta\delta y), \quad B_y = \frac{B_2}{2}(x_\beta^2 - y^2) + B_2 x_\beta\eta\delta + \frac{B_2}{2}(\eta\delta)^2,$$

So, to lowest, order they feel a dipolar perturbation and the gradient error

$$\Delta K_{x,y}(\delta) = \pm S\eta\delta.$$

Considering both the energy deviation-induced gradient errors and the sextupole gradient effect, we have a total error $\Delta K = (K - S\eta)\delta$ in eq. (2.21). The chromaticity in a lattice with sextupoles thus reads

$$\xi_{x,y} = \mp\frac{1}{4\pi}\oint \beta_{x,y}(K_{x,y} - S\eta)\mathrm{d}s,$$

which depends linearly on sextupole strengths, allowing for the correction of chromaticity to specified values. The cost of correcting chromaticity is the insertion of perturbations and nonlinearities in the dynamics.

2.7 Nonlinear Dynamics and Perturbations

Action-Angle Variables

Betatron motion of equation (2.11) can be obtained as Hamilton's equations for the effective, linear Hamiltonian

$$\mathcal{H} = \frac{1}{2}u'^2 + \frac{1}{2}K_u(s)u^2. \tag{2.28}$$

A transformation $(u, u') \to (\psi, J)$ to Action-angle variables is implicitly implemented by the type-1 generating function

$$F_1(u, \phi_u) = \int u'\,\mathrm{d}u = \frac{u^2}{2\beta_u}\left(\tan \phi_u - \frac{\beta_u'}{2}\right). \tag{2.29}$$

The action variable reads

$$J_u = -\frac{\partial F_1}{\partial \phi_u} = \frac{u}{2\beta_u}\sec^2 \phi_u = \frac{1}{2\beta_u}[u^2 + (\beta_u u' + \alpha_u u^2)], \tag{2.30}$$

from which we recover the pseudo-harmonic form $u = \sqrt{2\beta_u J_u}\cos(\phi_u(s) + \phi_0)$.

In the J, ϕ variables, the new hamiltonian is $H_0(\phi, J)$, given by

$$H_0 = \mathcal{H} + \frac{\partial F_1}{\partial s} = \frac{J}{\beta}. \tag{2.31}$$

Performing the change to action-angle variable in both the horizontal and vertical planes

we find the new Hamiltonian for 4D dynamics

$$H_0 = \frac{J_x}{\beta_x} + \frac{J_y}{\beta_y}, \tag{2.32}$$

and Hamilton's equations read

$$\phi'_u = \frac{1}{\beta_u(s)}, \qquad J'_u = 0. \tag{2.33}$$

Perturbations and tune-shifts

Linear motion is integrable, since it can be written in terms of the action variable only (angle-independent Hamiltonian). This leads to the action variable being a constant of motion, and the phase advance behaving just as the pseudo-harmonic motion anticipated.

Linear motion, though, is only a useful first approximation. In reality, in an storage ring, there are higher order multipole magnets, such as sextupole magnets, and also multipole, alignement and excitation errors, all acting as perturbations to linear motion. Generically referring to perturbations as $V(J, \phi)$, we can write the perturbed motion Hamiltonian

$$H(J, \phi) = H_0 + V(J, \phi). \tag{2.34}$$

Hamilton's equations read

$$\phi'_u = \frac{1}{\beta_u(s)} + \frac{\partial V(J, \phi)}{\partial J_u}, \quad J'_u = \frac{\partial V(J, \phi)}{\partial \phi_u}. \tag{2.35}$$

Since the tunes consist on the phase advance per revolution, we immediately see that the presence of perturbations leads to tune-shifts. Generically thus, the tunes can be expressed in terms of the tune-shifts as

$$\nu_0 = \nu_{u0} + \xi_u(\delta)\delta + \alpha_{uu}J_u + \alpha_{uv}J_v$$

where ξ_u represents the energy-dependent tune-shifts (higher order generalization of linear chromaticity), and the other components consist on the amplitude-dependent tune-shifts, up to first order in the actions.

Ressonances

4D linear unperturbed motion consists on the motion of two uncoupled parametric oscillators. The phase-space is diffeomorphic to the 2-Torus, $\mathbb{T}^2$, and there are an infinite number of such tori, corresponding to the different choices of initial conditions J_u.

Canonical perturbation theory applied to perturbed motion fails to converge

whenever the ratio of tunes is sufficiently rational. The Poincare-Birkhoff theorem states that under such conditions, almost all the periodic phase-space orbits disappear. An even number of tori survives, half of which are stable and half unstable. Unstable motion in a storage ring can eventually lead to beam loss.

The condition for sufficiently rational tunes can be expressed as

$$m\nu_x + n\nu_y = \ell,$$

for $n, m, \ell \in \mathbb{Z}$. This condition defines lines in tune-space corresponding to the locus in which perturbation theory fails and motion can become unstable. These are resonance lines and $|n| + |m|$ is the order of the resonance. Figure 2.6 shows resonance lines for the resonances up to second, third and fourth order respectively. First order resonances can be excited by dipolar fields, 2nd order resonances can be excited by quadrupole fields and 3rd order resonances can be driven by sextupolar fields.
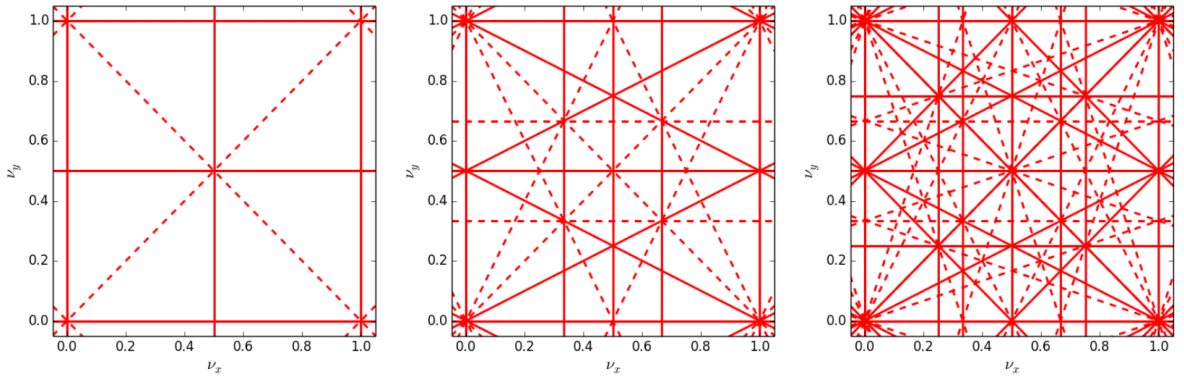
Figure 2.6: Resonance lines in tune space up to 2nd, 3rd and 4th order, respectively.

Dynamic Aperture

Nonlinear dynamics can become sensitive to initial conditions when the amplitudes are large. Because of the tune-shfits, specially the amplitude-dependent tune shifts, the tunes can wander in tune space, eventually crossing resonance conditions that may lead to instabilities, chatotic motion and beam loss. The dynamics can impose limitations to the maximum transverse deviations in which the beam can oscillate while displaying regular and bounded motion. This is a dynamic restriction to the motion known as the *dynamic aperture.*

Exceeding the dynamic aperture eventually leads to beam loss. During injection of the beam, if the transverse offsets are larger than the dynamic aperture, the beam is not captured into the storage ring. This is specially important for off-axis injection, such as in the case for SIRIUS.

CHAPTER 3

Online Optimization

This chapter defines, introduces and justifies online optimization in the context of accelerators. A bief overview of optimzation algorithms and their classifications is presented. The Robust Conjugate Direction Search (RCDS) algorithm is introduced as well as the other routines from which it was derived from.

This chapter adds no novelty to the literature in optimization. It is just an overview for merely pedagogic purposes. It is mostly based on the disscussion presented by the classic Numerical Recipes, as well as Refs.

3.1 Defining Online Optimzation

Suppose we have a machine (we do) in which there is some sort of figure of merit depending on the collective state of some set of relevent components, parts or operation modes–our parameters. There is no mechanistic/deterministic or probabilistic model for the dependence of the figure of merit on the reparameters state, but we do know the parameters affect the figure of merit. We may call these relevant parameters as knobs, since we can use them to tune the figure of merit.,

Now suppose we want to tune the knobs so the figure of merit reches a certain value, or so that it is minimized or maximized. This is an optimization problem, and we might as well call the figure of merit our objective function. Since the whole system is a black-box, to measure diferent values for the objective function, i.e., to sample it, we need to change the knobs and measure it again. The tuning procedure is thus based on trial-and-error.

If we are able to devise a computer-automated strategy to seek for the desired value or extremum of the objective function, then running this program while the machine is up and working is what we define as online optimization. The program must measure the objective function and read the current state of the knobs, calculate/decide and apply the changes on the knobs, measure the objective again and evaluate and judge the quality of the changes carried out. The process is iterated until the desired outcome is reached.

This black-box, heuristic optimzation problem describes the Dynamic Aperture otpimzation problem very well. The DA is a figure of merit related to the nonlinear

dynamics–in SIRIUS' case, the sextupole magnets. There is no analytical/statistical[1]
model prediciting DA changes given sextupole nudges so we cannot invert the problem
and tune sextupoles to A desired DA value. The tuning procedure must be based on
trial-and-error.

3.2 Justifying Online Optimization

Running online optimization in a machine will find the nearest extremum
(minimium/maximum). In other words, if no stochacity element is brought into the routine
to diversify the search along the parameter space, it will find local, not global extrema.
How can we be sure the local minima are the best solution for the optimization problem?

It seems that we will never know, but it actually does not matter. A good-
performing solution is all we care about as long as other operation parameters are not
affected (more details on the next chapter). But there are reasons to believe the local
minima found are actually the global ones and it has to do with how accelerators are
designed and the origins of deterioration of the dynamic aperture in the machine.

Because there are correction schemes for the linear dynamics in accelerators, the
Dynamic Aperture, i.e. limitations to the allowed oscillation amplitudes, arises because of
perturbations acting in a nonlinear dynamics. Other than that, the only limitation would
be the physical aperture[2]. The strength and symmetry of the whole magnets lattice is
decided based on simulating several possibile machine lattice configurations and evaluating
parameters such as the dynamic aperture and the beam-lifetime. The best performing
and viable solution (lattice) is implemented in the real machine.

In the real machine, additional errors arising from magnets misalignment or any
fields deviations can (and will) introduce additional perturbations and can deteriorate the
DA. The simulating procedure actually does take into consideration the existence of errors:
they are introduced in the model during evaluation of the figure of merit parameters and
the best performing lattice on average is chosen.

In the machine, a particular error configuration is physically realized, and we
are thus dealing with one possible lattice realization, for which the optimum configuration
is not that with the largest average DA or lifetime. But we expect it to be not too far
from that reference configuration chosen and applied to the machine. Online optimzaiton
thus consists on adjusting the sextupole lattice to the physically realized machine lattice
so that it reaches its best-performing configuration.

---

[1]in principle, a surrogate model could be trained to reproduce dynamic aperture given the sextupole
strengths as inputs. This is not what we have done so far

[2]Unperturbed nonlinear motion can display no limitations to oscillation amplitudes

3.3   Robust Conjugate Direction Search

Optimization routines and algorithms are usually classified according to whether they rely on the calculation of derivatives (gradient-based) or solely on the comparison of the objective function values (gradient-free). The latter can yet be classified into direct- or indirect-search methods, depending on whether the search of the extremum relies on direct comparisons of the objective function itself or from a mathematical model of it, respectively [?].

Both gradient-based and gradient-free strategies rely on the comparison of the objective function at different points of the parameter space. If the objective function suffers from noise this can significantly reduce the efficiency of the optimization routine [?, ?]. In Chap. 7 of Ref. [?], a review of the most popular optimization algorithms shows how most of them suffer to find minima to, at least, the precision of the noise-σ the objective function is subjected to.

The Robust Conjugate Direction Search (RCDS) algorithm is a indirect-search, gradient-free optimization algorithm introduced in Ref. [?]. The algorithm consists of a main loop for constructing and managing optimal search directions along the knobs space (Powell's Method) and a one-dimensional optimizer responsible for a noise-aware search for the minimum along a given direction. The algorithm is capable of optimizing the objective function (find its local maximum/minimum) to at least the precision of the objective-function noise [?, ?], being thus adequate for online optimization problems. Specifically, for accelerator controls and optimization, the algorithm has been successfully applied to optimize beam steering and optics matching during injection [?], reducing horizontal emittance [?, ?]and optimization of dynamic aperture [?, ?, ?, ?, ?].

RCDS actually consists on small modifications of well-known indirect-search routines. To grasp how it works, a brief overview on its predecessors is presented next.

3.3.1   Line methods

Let us incorporate the role of an accelerator operator and suppose we are seeking the configuration of a single knob rendering the best peformance, say, the minimum of a certain figure of merit. We nudge the knobs slowly and measure the objective, scanning for the minimum. We might scan tuning the knobs up while the objective goes downhill, and stop when starts increasing. The knobs lives over the real line, so this is basicaly a line-scan, the basis of line optimization methods. How to teach a computer do the same?

Let $f(x) \in \mathbb{R}$ be the objective function depending on the single parameter $x \in \mathbb{R}$. The task of optimizing f is achieved by a direct search over its domain. Since maximizing a function equals to minimizing the same function multipled by -1, in what follows, we shall refer to minimization only.

The search for the minimum is usually preceeded by initially *bracketing* the

miminum. We seek for points $a < b < c$ in the domain such that $f(b)$ is smaller than both $f(a)$ and $f(c)$. If f is reasonably smooth, we are certain there will be a minimium in the interval (a, c). Standard bracket routines for well-behaved, noiseless objective functions can be found in the literature, and mostly consists on, starting from an initial point, scanning the line "downhill" until the function stops decreasing.

We can see the bracketing procedure as a coarse-grained scan initially performed by the operator. The minimum is then finely searched on a second line-search scan. Given an intial bracketed interval, the most common line-search methods are

- Golden Section Search: which progressively scans within the brackets, updating it at each iteration so that it shrinks at each round until it spans only a small interval specified by the user. The machine precision ϵ is often indicated. The guess for the miminum is taken as the mid-point along the interval. The minimum point is found to within the precision of $\epsilon/2$.

- Parabolic Interpolation: where a parabola is fitted to the values $f(a), f(b), f(c)$ the function takes along the brackets. Moving along the parabola minimum takes us to f's minumum or pretty close to a it in a single leap.

The brackets routine and the line-search methods presented rely on the comparison of the objective function at different points in the parameter space. They assume the functions to be deterministic and trust the behaviour and are completely unaware of the experimental noise.

In what follows, we assume what we actually measure in the control-room is $\hat{f}(x) = f(x) + \xi$, where $\xi \sim \mathcal{N}(\mu = 0, \sigma)$ is a random variable modeling the experimental noise, with σ being expected noise error, $\sigma^2 = \mathrm{Var}[\xi]$.

For the optmization of noisy objective functions, RCDS introduces a noise-aware bracketing routine and a parabolic interpolation scan over the bracket interval. For the brackets, instead of seeking for points $a < b < c$ satisfying $f(b) < f(a), f(b) < f(c)$, RCDS requires a more strict condition $f(b) < f(a) + 3\sigma, f(b) < f(c) + 3\sigma$. This increase the likelihood the observed trend consists on real trends of the objection itself, rather than random errors.

During the line-search, a parabola is fitted within the brackets and its minimum is taken as the objective function minimum. Additionally there is a comparison of the available (previously evaluated) points within the brackets used for the fitting of the parabola. If any of them is considered an outlier, it is discarded and the fitting is repeated without it.

bracketing and linescan illustrations
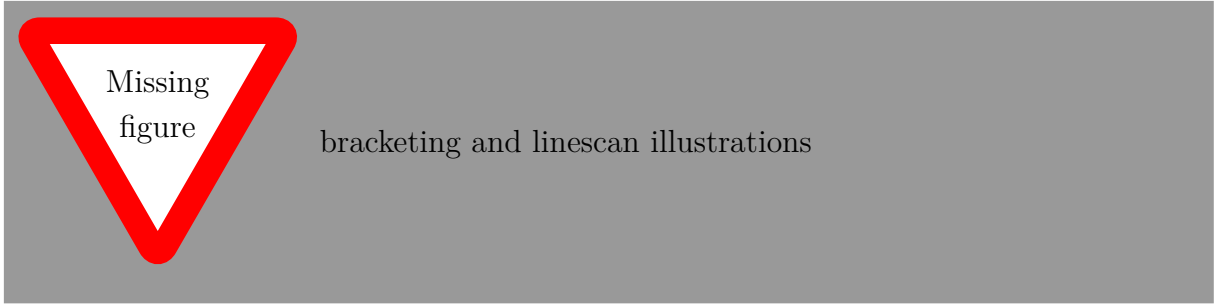
3.3.2 Powell's conjugate direction set

How could we optimize an objective function $f(\mathbf{x}) \in \mathbb{R}$ depending on the set of p parameters $\{x_i\}_{i=1,\ldots,p}$? The simplest idea is to iteratively optimize nudging each knob individually: optimize f by changing x_1, while the other knobs remain fixed. Next, optimize by changing x_2 only, and so forth. In other words, each one of the knobs defines a direction whose basis vector is $\hat{\mathbf{e}}_i$, correspoinding to a unit change of the knob. This is easy to automate with the noise-robust line-optimzer introduced in the previous section.

Formally, we are reducing a multi-dimensional optimzation problem into a series of line-searches. That is, given an intial configuration of the parameters (an initial position) $\mathbf{x}_0$, and a direction $\hat{\mathbf{n}}$, we have the one-dimensional problem to minimize $g(\delta) = f(\mathbf{x}_0 + \delta\hat{\mathbf{n}})$. The minimum is then $f(\mathbf{x}_0 + \delta_*\hat{\mathbf{n}})$, where $\delta_* = \arg\min_\delta g(\delta)$. In the previous paragraph, we specialized to $\mathbf{n} = \hat{\mathbf{e}}_i$, and iterated for $i = 1, \ldots, p$.

basis vectors minimization vs conjugate directions
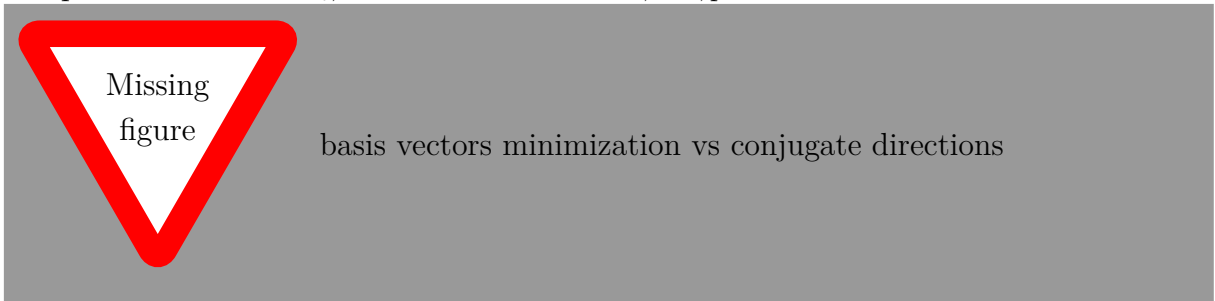
As can be seen in figure, scanning along each orthogonal directioon can be time-consuming, specially for some functions with long narrow valleys at some angle with the coordinates basis vectors. This strategy thus is suboptimial when evaluation of the objective function is expensive.

The reason why using unit basis vectors can be so inneficient is because optimizing along a given basis vector spoils down minimization carried out in the any other of them. So the processes needs to be iterated. A more efficient strategy consists on constructing a set of special non-interfering direction vectors for which the minimizationsare preserved when optimizing in a different driection.

The necessary condition for direction vectors $\mathbf{u}$ and $\mathbf{v}$ to be non-interfering is (proof in the apendix)

$$\mathbf{v} \cdot \mathbf{H} \cdot \mathbf{u} = 0, \tag{3.1}$$

where $(\mathbf{H})_{ij} = \partial^2 f(\mathbf{x}_0)/\partial x_i \partial x_j$ is the Hessian matrix for function f. The $\mathbf{u}$ and $\mathbf{v}$ directions are said to be conjugate directions.

The problem now consists on finding an appropriate set of p conjugate directions, so we can optimize $f(\mathbf{x})$ along them. Let $\{\mathbf{u}_i\}$ denote our directions set. Powell proved conjugate directions can be constructed as follows

1. Set the initial directions as the basis vectors: $\hat{\mathbf{u}}_i = \hat{\mathbf{e}}_i, i = 1, \ldots, p$.

2. Save the starting point (initial parameters state) as $\mathbf{x}_0$;

3. For $i = 1, \ldots, p$ minimize along $\hat{\mathbf{u}}_i$. Save the minimimum as $\mathbf{x}_i$.

4. For $i = 1, \ldots p - 1$ set $\hat{\mathbf{u}}_i \leftarrow \hat{\mathbf{u}}_{i+1}$

5. Set $\mathbf{u}_p = \mathbf{x}_p - \mathbf{x}_0$. Normalize to obtain $\hat{\mathbf{u}}_p$.

6. Minimize along $\hat{\mathbf{u}}_p$. Name the found minimum as the new $\mathbf{x}_0$ and repeat the procedure until reaching a certain number of evaluations or until some stopping condition is reached.

That is, from steps 1–3. we optimize along each one of the unit basis vectors, updating the minimum. When finishing optimization along x_p, the current minimum will be $\mathbf{x}_p$. In step 4 we discard the first direction, rename directions $\mathbf{u}_{i+1}$ to $\mathbf{u}_i$, and set as our new pth direction the vector from the starting point $\mathbf{x}_0$ to the the current minimum.

Powell proved that repeating this procedure k times for a quadratic form produces a set of directions whose last k vectors are mutually, pairwise conjugate, in the sense of the Hessian matrix. So p iterations exactly minmizes the quadratic form. The method is also quadratically convergent: each iteration doubles the number of significant figures of the candidate minimum for the quadratic form.

There is a problem in throwing away for $\hat{\mathbf{u}}_1$ for $\mathbf{x}_p - \mathbf{x}_0$ every iteration: at some point the lines start to fold up on each other and lose linear independence. As a result the function can end up minimized only within a subspace of parameter space. To fix this, you can reinitialize the directions to the basis vectors after an iteration along the p directions, or use any new set of orthogonal directions.

The somewhat counterintuitive solution suggested by Powell is to discard not necessarily $\hat{\mathbf{u}}_1$ in favor of the new direction, but the direction along which f had its largest decrease so far. This is justified because this direction is likely have a largest component along the new proposed conjugate direction. Accepting this advice results in a set of p directions which are no longer mutually conjugate by the end of p iterations. As a result, the method will no longer be quadratically convergent

Powell also posits some conditions in which is best not to add any new directions, keeping the old set from the previous iteration. These are presented in the appendix, as well as the pseudo-code for the Powell loop.

In summary, Powell's direction set loop calculates and manages directions adaptatively, deciding when to change old directions in favor of newly calculated conjugated vectors, and when to avoid the changes to control build-up of linear depencence

In practice, using conjugate directions accounts to finding a good set of directions in which the number of steps along the vectors is reduced. They provide "shortcuts" towards the minimum in the objective landscape.

CHAPTER 4

Dynamic Aperture Optimization Experiments

This is a "methods" chapter. Its first section presents the available diagnostics at the storage ring and describes the experimental measurements of relevant quantities such as beam positions, trajectories and orbits, beam current and lifetime, the tunes and chromaticity and how these are dialed at our will during a study. The other two sections discuss the choice of objective functions to probe the Dynamic Aperture and the appropriate selection of sextupoles to act as knobs.

4.1 Diagnostics and measurements at the control room

4.1.1 Beam Position Monitors

Beam-position-monitors (BPMs) consist on a set of four antennas placed inside the vaccum chamber. The antennas are placed in such a manner that when the electron beam passes through it, it induces mirror charges which trigger the antenna a certain voltage. The singal from the antennas is electronically processed allowing for the inference of relative changes in the beam's centroid position. BPMs thus record the average beam's relative trajectories changes along the transverse plane.

BPMS antennas diagram

4.1.2   Beam-Current Monitors

DCCTs allow us to measure the stored current on the ring. From the current in the booster or the transport line immediately before the injection into the storage ring and the measurement of the storage ring stored current immediately after we can infer the efficiency of the injection process.

4.1.3   Tunes monitor & tune changes

When turn-by-turn motion is viewd at a fixed s position, it consits on the sampling of harmonic motion. The fundamental frequency is the tune ν. Precise measurement and monitoring of the tunes is achieved by placing a stripline, which constantly excites the beam in a narrow range of frquencies. The freuqency which is capable of exiciting a resonance peak is idnetified as the tune

As for changes and control of the tunes, as formula () reveals, changes in the quadrupoles, specially at large β-function sections allows for the control of the tunes. In fact, knowing the response is linear, a tune-response matrix can be constructed, i.e. the Jacobian of the tunes with respect to changes in quadrupoles

$$\Delta\boldsymbol{\nu} = \mathbf{J}_{\nu}\Delta\mathbf{K}, \tag{4.1}$$

where $\boldsymbol{\nu} = \begin{bmatrix} \Delta\nu_x & \Delta\nu_y \end{bmatrix}^{\mathsf{T}}$ and the Jacobian has matrix elements

$$(\mathbf{J}_{\nu})_{ij} = \frac{\partial\nu_i}{\partial K_j} \approx \frac{\Delta\nu_i}{\Delta K_j}, i = x, y. \tag{4.2}$$

The system can pseudo-inverted allowing for the determination of quadrupoles changes for a desired tune change.

4.1.4   Chromaticity changes & measurements

Chromaticity corresponds to the tune change per unit change in the relative energy deviations δ. In practice, to we calculate the tune changes per unit RF cavity frequency changes.

Due to the lienariry of the problem, chromaticity is corrected or changed according to the same pseudo-inversion procedure described above for the tunes. We relate chromaticity changes to sextupole changes

$$\Delta\boldsymbol{\xi} = \mathbf{J}_{\xi}\Delta\mathbf{S}, \tag{4.3}$$

Need to study it

needs re-fresh-ing

where $\boldsymbol{\xi} = \begin{bmatrix} \Delta \xi_x & \Delta \xi_y \end{bmatrix}^{\mathsf{T}}$ and the Jacobian has matrix elements

$$(\mathbf{J_{\xi}})_{ij} = \frac{\partial \xi_i}{\partial S_j} \approx \frac{\Delta \xi_i}{\Delta S_j}, i = x, y. \tag{4.4}$$

and carry-out the pseudo-inversion. In practice, though, the chromaticity jacobian was never actually calculated in the real machine, due to the time-consuming process of varying a single sextupole family, carrying out the chromaticity measurement and repeating it for the 21 families. The SIRIUS computer model is used to construct the matrix and whenever a chromaiticity change is desired or required, the changes are calculated by pseudo-inversion of the model-calculated Jacobian

4.2   The choice of objective function

There is no analytical formula for relating the storage ring linear or nonlinear optics to the Dynamic Aperture. The optimization procedure must be a direct search procedure: changes are performed in the knobs and the effect over dynamic aperture is evaluated.

Also, we cannot measure dynamic aperture directly. We must choose an objective function to act as a probe to the DA: a figure of merit related to the dynamic aperture to represent it.

Two objectives usually adopted as probes are the injection efficiency and the beam's resilience to dipolar perturbations. The former is quite self-explanatory: the larger the dynamic aperture, the larger space for the beam to be captured during injection, and thus the larger the injection efficiency. The latter is related to the DA by the following: the larger the horizontal dipolar kicks the beam can survive, the larger the orbit distortions towards the positive or negative horizontal plane (depending on the kick direction). So the larger the amplitudes the beam explores as it oscillates, probing the DA borders. If the beam survives to large kicks, it means the ring can accomodate larger orbit distortions because of an increased dynamic aperture .

In summary, the dynamic aperture optimization procedure must consist on the exploration of sextupole (knobs) configurations yielding the largest dynamic aperture as accessed by as objective function such as injection efficiency or beam kick-resiliency.

4.2.1   Injection scheme for acummulation at SIRIUS storage ring

Beam acummulation into the storage ring occurs in the off-axis scheme. The beam is delivered at $x \approx -8$ mm, and receives the kick from the nonlinear kicker field. The field profile is nonlinear, with zero field and gradient at the center of the axis, so that it does not disturbs the stored beam. In the off-axis scheme, a sufficiently large dynamic

aperture is desired to allow the beam to be captured into the storage ring. The predicted efficiency for SIRIUS setup, considering a dynamic aperture reaching $x = -9$ mm, was nearly 100%. What was observed during 2022 was an injection efficiency of about $88 \pm 8\%$.

4.3   Selection of optimization knobs

The dynamic aperture is determined by the quality of the dynamics in terms of perturbations and nonlinearities. Considering corrected quadrupoles and dipoles (linear optics), the main factors influencing SIRIUS DA are the nonlinearities introduced by the sextupoles and possbibly their field's small errors and deviations from the design parameters. The goal, thus, is to search for the sextupole configurations rendering the largest DA.

The sextupoles are the parmeters which can be tuned, the knobs. SIRIUS has 21 sextupole families: magnets powered by the same power supply. 6 of them are achromatic sextupoles. They are placed where the the dispersion is zero. The 15 other families are chromatic families. Table 4.1 shows the 21 sextupole families names. In

Table 4.1: SIRIUS sextupole families

achromatic	SFA0, SDA0, SFB0, SDB0, SDP0, SFP0
chromatic	SDA1, SFA1, SDA2, SFA2, SDA3, SDB1, SFB1 SDB2, SFB2, SDB3, SFP1, SDP1, SDP2, SFP2 SDP3

principle, thus, the optimization parameter space is 21-dimensional. In reality, we would like to change sextupoles without changing chromaticity. Since we need at least one degree of freedom for correcting chromaticity in the horizontal plane and one degree of freedom for correcting the chromaticity in vertical plane, there are 19 available knobs. The dimensionality of the search space can be further reduced by imposing additional constraints to certain families variations. The specific choices of knobs for optimzation experiments are discussed in more details in the Results section.

4.3.1   Characterization of Sextupole Magnets Configurations

Once a configuration of sextupoles (position in parameter space) is found, the nonlinear optics it provides the machine needs to be characterized. The characterizations consisted on evaluatig/measuring the followint figures of merit and desired features

- Injection efficiency in nominal off-axis conditions : this is the most desired characteristic. The sextupoles are to be optimized so the DA and the off-axis injection efficiency increase.

- Beam Kick resilience: a small current of 2 mA, concentrated in a single bucket is stored in the ring. The beam is kicked by the horizontal dipole kicker, which instantly provides a dipolar perturbation leading the beam to be displaced in the horizontal direction. The current before and after the kick is recorded by a current monitor (DCCT) and allows for the calculation of the fraction of the beam lost as a consequence of the kick and the transverse displacement. The procedure is repeated with progressively stronger kicks, and a curve of beam loss as a function of the kick can be constructed. The smaller the losses for larger kicks, the larger the resilience.

- Phase portrait area: it is expected that the optimzation procedure increases the dynamic aperture of the machine, meaning it can accomodate larger oscillations and larger phase portraits $x - x'$. Using beam position monitors (BPMs) at the two ends of a straight section, which record the positions of the beam centroid at each turn, we can calculate the position and angle of the beam in the middle of the straight section, and thus recostruct the phase-portrait from turn-by-turn (TbT) data.

- Beam lifetime: the lifetime at SIRIUS is dominated by losses due to electron-electron interactions leading to momentum transfers exceeding the energy/momentum acceptance (MA). Optimization of DA does not necessarily leads to improvements in the MA. If the MA is reduced, the rate at which the beam is lost can increase, reducing the total lifetime. It is desireble that the configurations found during DA otpimzation do not worsen the MA and beam lifetime considerably.

- Chromaticity: Sextupoles are introduced in the storage ring for correction of focusing chromatic aberretions. When changing the sextupole settings, it is desired to do so in such a manner that the chromaticity is unchanged. The methods for choosing the optimization knobs already take into account the need for keeping constant chromaticity. Still, after optimization is performed, we need to check whether chromaticity is unchanged.

The first two characterizations are quite similar to the two most immediate objective function candidates mentioned above. Indeed, in most nonlinear dynamics optimzation experiments, optimization using injection efficiency or kick resilience as objectives seemed

to be completely interchangable. Improvements in injection efficiency necessarily led to improvements in kick resilience, and vice-versa. As shown in more details in the results section, for the SIRIUS storage ring this appears not to be the case. The configurations can be specialized to improvements solely on injection efficiency or solely to kick resilience. This feature was observed during the characterization of the optimized sextupole settings with respect to these two figures of merit.

CHAPTER 5

Experiments and Results

This section presents partial results from the optimzation experiments carried out up until now. The early experiments were performed in december 2022, and the latest have been happening since february 2023.

5.0.1 Kick resilience optimization - december 2022

The parameter space (knobs) adopted consisted on the SDA0, SDB0, SDP0, SFA0, SFB0, SFP0, SDA1, SDB1, SDP1, SDA3, SDB3, SDP3, SFA1, SFB1, SFP1 sextupole families. The SDA2, SDB2, SDP2 and SFA2, SFB2, SFP2 families were used keep chromaticity constant when varying the optimization knobs. This was implemented in the following manner: RCDS freely proposed strength variations to the knob families. For each proposed change in strength, the corresponding changes in chromaticity were estimated from a chromaticity jacobian matrix constructed from the model. To the "correction" families were applied the strengths needed to cancel these chromaticity changes. In this first attempt, we tested the optimization routine twice, with different objective functions to probe the dynamic aperture.

- Objective function: kick resilience
  The first objective function adopted was the beam loss after dipolar kick from the horizontal dipole kicker. The idea was to minimize the loss at a given kick, and progressively increase the kicks, to probe larger acceptances. The BPMs acquisition was fired in synchrony with the dipole kick and beam-loss was calculated by comparing the sum-signal[1] of the beam's first 10 turns with the sum-signal of the last 10 turns. As for the strength of the dipole kick, we set a horizontal kick of $\Delta x' = -0.760$ mrad, which rendered about 35 - 40% of beam-loss.

- Experiment:
  With the aforementioned scheme for changing strengths in the sextupole families, RCDS was started to minimize the beam-loss upon the horizontal kick. In the

---

[1]BPMs determine the relative changes in position of the beam centroid from the differential image charges the beam induces in the device's four antennas. The sum-sginal consists on the sum of the signal from all the antennas and, up to a scale, represents the total beam current. Relative changes in sum-signal correspond to relative changes in beam current.
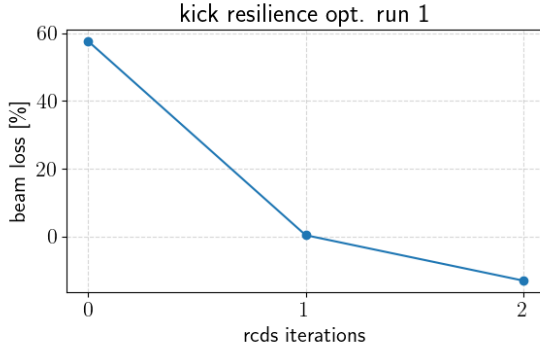
Figure 5.1: Objective function history vs. iterations of the first trial at beam-loss optimization.
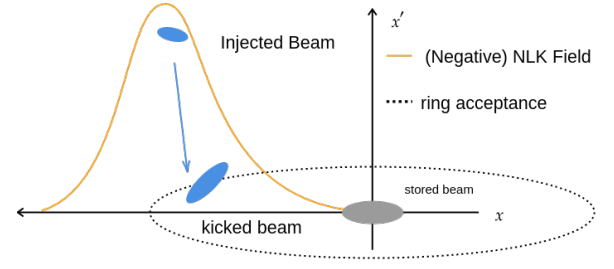

Figure 5.2: Injection conditions for DA optimization

algorithm's first iteration[2], beam loss dropped from 60% to nearly 0% (Figure 5.1). In the beginning of the 2nd iteration, the objective function took negative values (an artifact) and we stopped the optimization run.

- Results:
  The beam-loss minimization significantly improved the beam's resiliency to dipole kicks. After the optimization, it was necessary to kick the beam at approximately $\Delta x' = -0.850$ mrad to achieve the same 30–40% beam-loss rate previously achieved by a $\Delta x' = -0.760$ mrad kick. By the end of this first attempt, the machine magnets were cycled[3] and the configurations found during optimization were loaded. When trying to inject in the nominal off-axis scheme, the efficiency was quite low. The improved kick resilience, however, was preserved. This raised the suspicion that the aperture along the negative horizontal direction might have been negatively impacted by the procedure, while the aperture in x' increased. This observation motivated the adoption of injection efficiency to probe the DA.

5.0.2   Injection efficiency optimization - december 2022

The first attempt at optimizing DA by minizing beam-loss revealed that the optimization procedure did not improve injection efficiency. We started another attempt, using the injection efficiency itself as objective function. The knobs (parameter space) used were the same as in the beam-loss optimization.

- Objective function & setup:
  The off-axis injection efficiency was worsened by reducing the NLK strength so the

---

[2]An RCDS iteration is reached upon completing the one-dimensional optimization along all directions in the parameter space. After each iteration, the algorithm constructs a new (conjugate) direction according to Powell's method and may replace existing directions by this new conjugate direction.

[3]Cycling or standardizing magnets cosnsists on driving their power suplies with decaying sinusoidal waveforms to remove hysteresis effects and bring the magnets yokes to their standard reference magnetization.
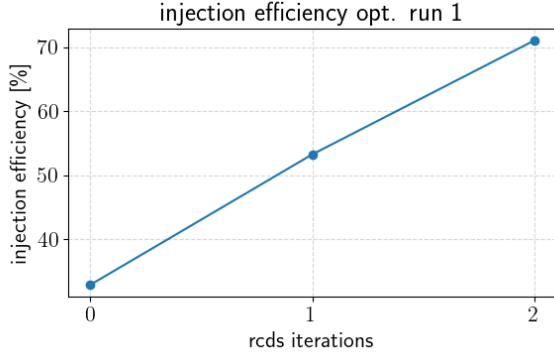
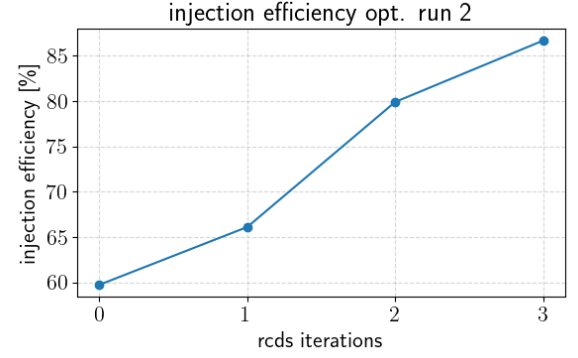Figure 5.3: Objective function vs iterations during the first run of injection efficiency optimization

Figure 5.4: Objective function vs iterations during the second run of injection efficiency optimization

beam was injected in the upper-left border of the (x, x') aperture (see Figure 5.2). The efficiency under such conditions was about 30%. The maximization of injection efficiency under such injection conditions should correspond to a maximization of the DA evenly among the x and x' directions, as opposed to the increase on the x' direction only, as seemed to be the case in the previous attempt.

- Experiment:

  In the first run, within three iterations the injection efficiency reached 70%, as shown by Fig. 5.3. The algorithm stopped as it reached the maximum number of the objective function evaluations. A second run was launched, starting from the sextupole configurations just found in the first ruun. In four iterations, 85% efficiency was reached, as Fig. 5.4 shows.

- Results:

  When the NLK strength was restored to the reference value, meaning the nominal off-axis injection conditions were restored (in which the beam "lands" not at the border but within the acceptance), the injection efficiency fluctuated around 95–100% with good repeatability. There was a severe reduction in beam lifetime by the end of the last optimization trial. Measurement indicated 54.12 hrs lifetime at 15 mA current, while, the reference (non-optimized) configuration, lifetime at this same current is about 68 hrs.

  We carried out chromaticity measurements in the machine loaded with the reference configuration (ref-config) and with the sextupole configurations found at iterations 0, 2, and 3 of the last injection efficiency optimization run (run shown by Fig. 5.4). Table 5.1 presents the measured values, from which we can note the chromaticity changes despite the efforts to anticipate and compensate them when applying changes to the sextupoles. It was later realized, due to the success of the optimization experiments throughout 2023, that the undesired changes in chromaticity are probably not related to this compensation scheme

itself, but rather by the choice of sextupole families operating close to their saturation strengths. Under such conditions, the applied fields are not repeatable, and the excited fields might not correspond to the correct values required to control chromaticity.

machine configuration	ξ_x	ξ_y
ref-config	2.33 ± 0.02	2.531 ± 0.008
iter 0	2.59 ± 0.02	3.700 ± 0.008
iter 2	2.72 ± 0.04	3.704 ± 0.008
iter 3	2.76 ± 0.05	3.510 ± 0.01

Table 5.1: Chromaticity measurements for ref-config and sextupole configs. found at the second round of injection optimization

In summary, in these early attempts in december 2022 it was realized that beam-loss minimization/kick resilience maximization does not necessarily leads to injection efficiency improvements. The $x - x'$ phase space seems to be "elastic" and the dynamic aperture can be deformed preferably along x or x' directions, rather than being uniformily increased, as the experiences in other accelerators suggests.

The injection efficiency optimization was successful, but at the expense of a significant decrease in beam lifetime. Undesired chromaticity changes were also observed.

5.0.3   Optimization experiments throughout 2023

In 2023, optimzation experiments were carried in the machine configurations with the nominal tunes $(\nu_x, \nu_y) = (49.08, 14.14)$, Working Point 1, as well as in the $(49.20, 14.25)$ and $(49.16, 14.22)$ tunes, Working Points 2 and 3 (WPs 1, 2, 3). Results reported here have also been presented in Ref. [?] (on WPs 1 and 2) and on the presentation delivered at the Optics Tuning and Corrections for Future Colliders Workshop.

The major differences from the previous experiments consisted on

- the use of the average injection efficiency of 5 injection pulses at 2 Hz objective function to reduce the experimental noise sigma from $\sigma = \pm 8\%$ to $\pm 1\%$.

- Families SFP1 and SFB1 were not used as knobs in the otpimzation experiments since they operate close to their saturation strengths, where hysteresis effects become significant.

- Knobs selection was based in choosing linear combinations spanning null space of the chromaticity response matrix for Working Points 1 and 2. See Ref. [?] for details. Working Point 3 knobs were chosen as described in section 9.1.

Optimization in Working Point 1

Three configurations were found, which resulted from optimizing the objective, loading the best configuration found and continuing the optimzation from the previous run's best.

For each one of the best configurations found during runs 1, 2 and 3 and also for the non-optimized reference configuration (ref. config.), turn-by-turn (TbT) BPM data of the stored beam kicked with the horizontal dipolar kicker were acquired. The DCCT current monitor allowed the determination of the current losses as a function of the horizontal kicks, which is shown by Figure 5.5. TbT data also allowed for the reconstruction of the (x, x') phase space of the beam under the influence of the kicks. Using two BPMs at the ends of an empty ID straight section, the position and angle of the beam were determined at each turn. Figure 5.7 shows the measured phase spaces for the ref. config. and the best configurations found during run 1, 2, and 3, at the fifth straight section (SA05), which is a high-beta section with identical optics to the injection point. In the measurement, the beam was under the influence of kicks rendering approximately the same current loss of 12%.
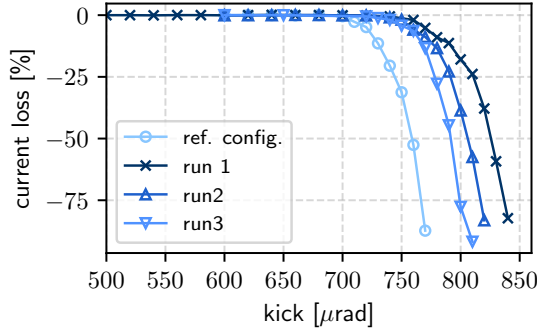

Figure 5.5: Current losses vs. horizontal dipole kick for the ref. config. and for the RCDS solutions at WP 1.
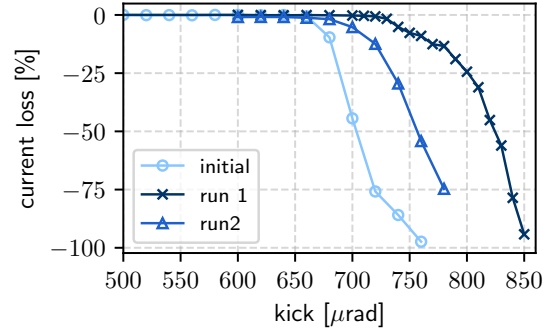
Figure 5.6: Current losses vs. horizontal dipole kick for the initial configuration and the RCDS solutions at WP 2.

Table 5.2 compiles the injection efficiencies (IE) achieved for each configuration during off-axis NLK injection in normal injection conditions ($x \approx -8.5$ mm, $x' \approx 0$). Again we stress that the point regarding the maleability of the phase portrait ellipses deformations: the configuration with the largest kick resilience, that of run 1, is not the one with the largest phase space area and IE performance. This could be explained if the phase space deformations of the ellipse at the kicker location for this sextupole setting resulted in a larger x'/x ratio, which would account for a larger kick acceptance and the worse injection performance compared to run 2.

Lifetime at 60 mA was measured at 20 hr for run 2 best configuration. Lifetime at the same conditions for the reference configuration is 21 hr. No significant chromaticity changes were observed: $(2.33, 2.53)$ in ref. config. vs. $(2.24, 2.39)$ in run 2 best solution.
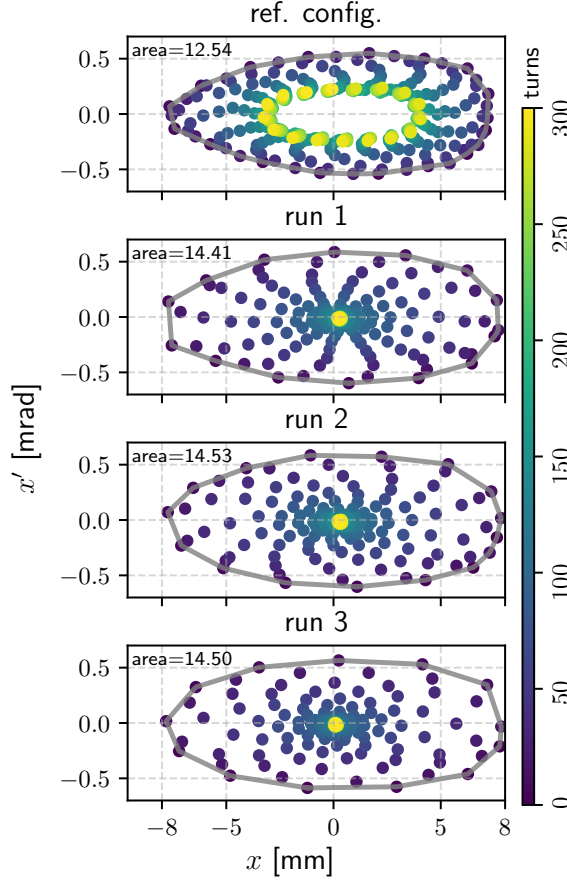
Figure 5.7: Measured phase space at SA05 high-beta straight section for the ref. config. and the best RCDS configurations of runs 1, 2 and 3 in WP 1. Color-map indicates the turns. The areas are in mm mrad. The beam was being kicked horizontally at 730 µrad in the ref. config, 790 µrad in run 1, 780 µrad in run 2, and 770 µrad, in run 3. Loss rates of 12%, 11%, 13% and 13%.
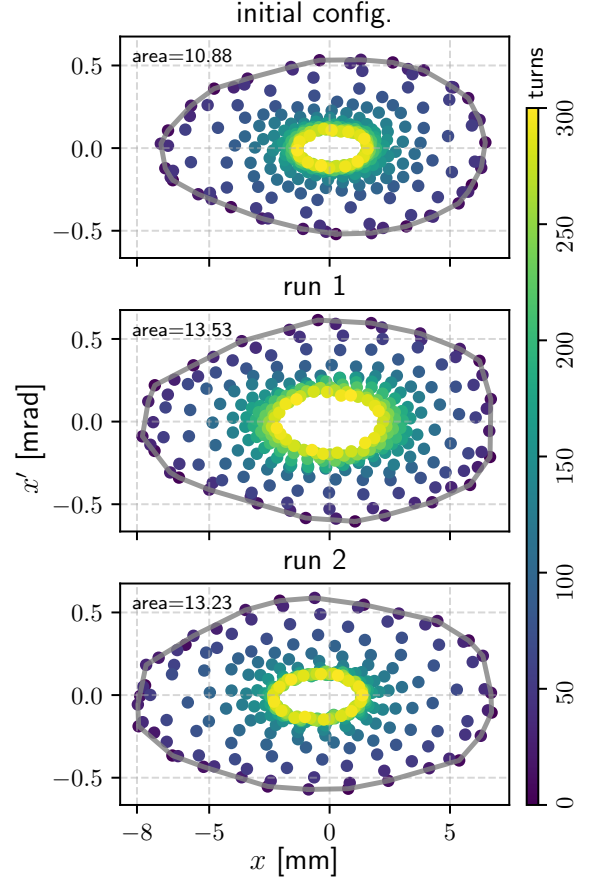
Figure 5.8: Measured phase space at SA05 high-beta straight section for the initial configuration and the best RCDS configurations of runs 1 and 2 in WP 2. Color-map indicates the turns. The areas are in mm mrad. The beam was being kicked horizontally at 680 µrad, for the initial configuration, 770 µrad for run 1, and at 720 µrad for run 2. Loss rates of 10%, 12% and 12%, respectively

Optimization in Working Point 2

In working point 2, two configurations were found: Run 1 and Run 2. The sextupoles were optimized from scratch from a configuration with the new tunes and then, from the best solution found, another round was launched.

TbT BPM data of the kicked stored beam in the initial configuration (non-optimzed) and in each run's best solution was acquired and allowed the determination of current losses vs. kicks, shown in Fig. 5.6, and the reconstruction of phase space, shown in Fig. 5.8. Table 5.2 compiles injection efficiencies achieved for the configurations in the new tunes during nominal off-axis injection. The configuration found during run 1 rendered the best IE, the largest kick resilience, a larger lifetime than the initial configuration (21 hrs, run 1 vs. 18 hrs, initial, at 60 mA), and the largest phase-space area increase.

Table 5.2: Injection efficiencies (IE) for configurations found for Working Points 1, 2 and 3.

working point 1		working point 2		working point 3	
configuration	IE [%]	configuration	IE [%]	configuration	IE [%]
ref. config.	88 ± 8	initial	51 ± 1	initial	
run 1	91 ± 1	run 1	79 ± 3	optimized	93 ± 3
run 2	98 ± 1	run 2	65 ± 1		
run 3	87 ± 3				

Optimization in Working Point 3

Two optimization runs were carried out, starting from sextupole settings of the reference configuration of the nominal tunes. Best configuration found at run 1 was loaded and run 2 was launched. The resulting configuration displayed injection efficiency of $93 \pm 3\%$ during nominal off-axis injection. Lifetime at 60 mA was measured at 19.5 hrs, so no significant reductions were observed.
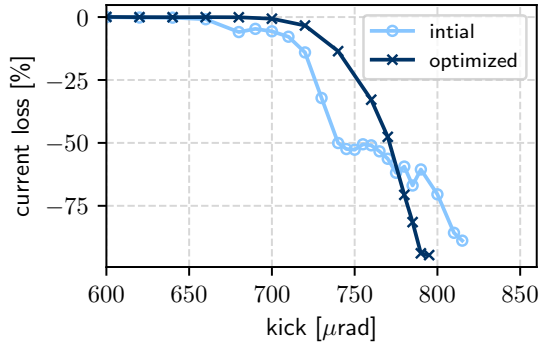
Figure 5.9: Current losses vs. horizontal dipole kick for the initial configuration and the RCDS solution at WP 3

Figure 5.10: Measured phase space at SA05 high-beta straight section for the non-optimized configuration and the best RCDS configuration in WP 3. Color-map indicates the turns. The areas are in mm mrad.

Orbit stability improvements were confirmed by the orbit integrated spectrum density, which decreased by a factor of approximately 2 [?]. Orbit rms variations reached

the record values of less than 1% of the horizontal beam size, in the horizontal plane, and less than 4% of the vertical beam size in the vertical plane.

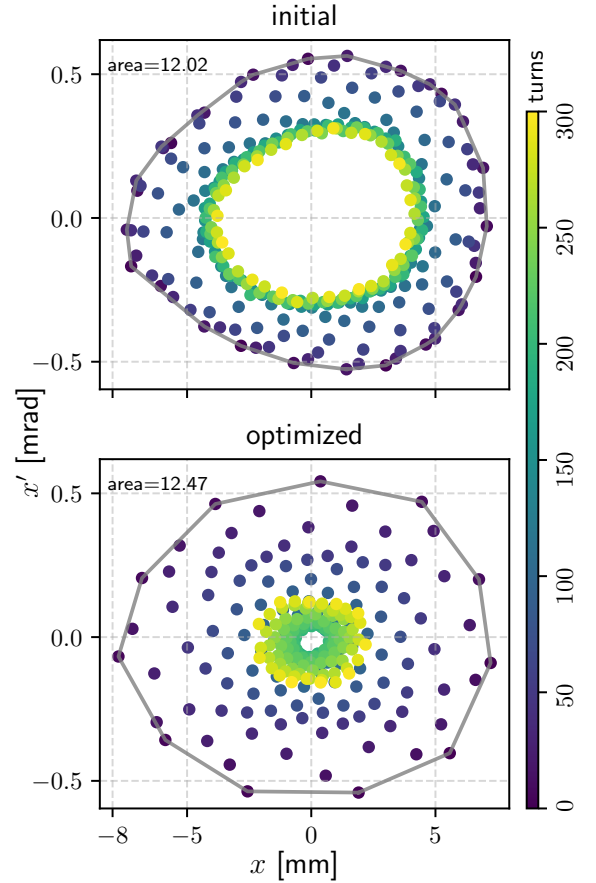In summary, in the experiments throughout 2023, the noise in the objective function was reduced and the injection efficiency average was established as the standard objective. No significant chromaticity changes were observed during/after the optimization runs, nor significant changes to beam lifetime, compared to the nominal working point reference configuration.

Excellent configurations were found in WP1, with 98% injection efficiency, but we still believe there is room for further improvements in the higher tunes configurations.
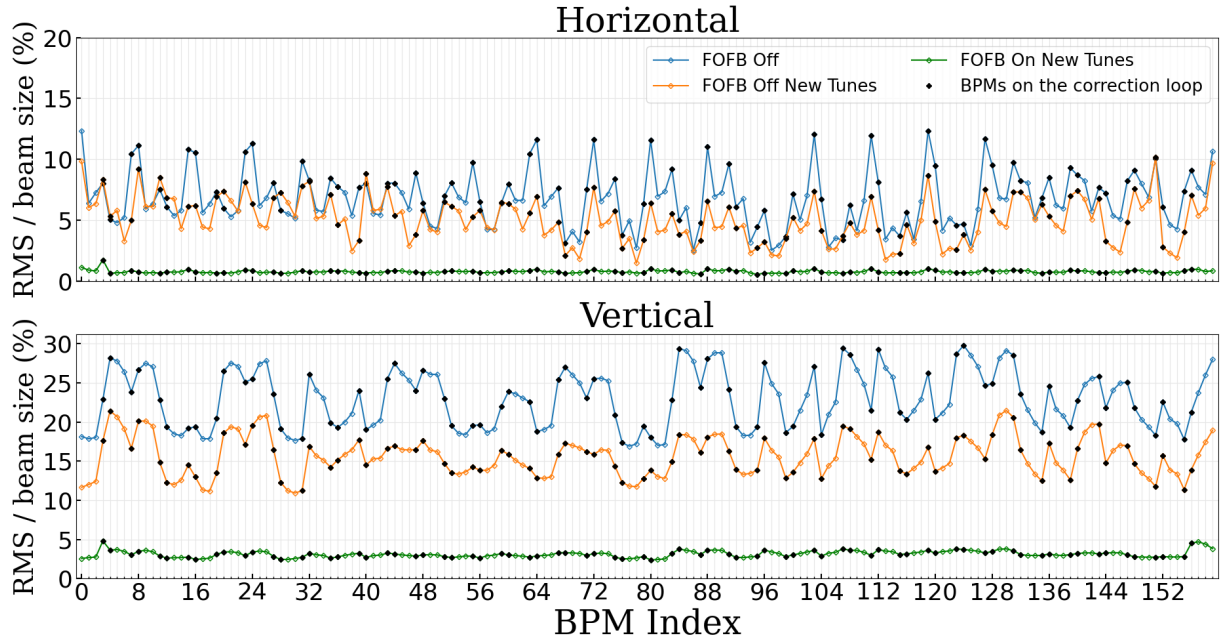

Figure 5.11: Horizontal/Vertical RMS orbit variations in units of the horizontal and vertical beam sizes. Blue curves represents variations in the nominal working point, WP1, orange curves are the orbit variations at WP3, and green curves variations at WP3 plus results of the recent improvements in Fast Orbit Feedback System. From [?]

5.1 Conclusions

The MSc. project is being developed on shcedule and should be completed within the stipulated duration of the grant. In the reported period from August 2022 to July 2023 the student has completed the graduate program requierements for course credits, co-athoured and collaborated in the writing of computer code for performing machine experiments, participated in the experiments and performed all the analysis of the obtained data. The student has also co-authored and submitted contributions to IPAC'23, the largest conference in the field of particle accelerators, and presented the results achieved so far during the project in the Optics Tuning and Corrections for Future Colliders Workshop, at CERN.

The work developed alongside the LNLS Accelerator Physics Group has contributed to the recent achievements of record orbit stability at the SIRIUS storage ring.

More experiments for further optimzation, exploration of working points and and characterizations of nonlinear dynamics performance should proceed in the upcoming months up until the end of the year, when the student should then focus in the writing of his dissertation.

CHAPTER 6

Discussion and Conclusions

Bibliography

[1] Wiedemann, H. *Particle Accelerator Physics.* Graduate Texts in Physics (Springer International Publishing, Cham, 2015). URL http://link.springer.com/10.1007/978-3-319-18317-6.

[2] Huang, Z. Brightness and Coherence of Synchrotron Radiation and FELs. *Free Electron Lasers* (2013).

[3] Hettel, R. Challenges in the Design of Diffraction-limited Storage Rings. *Proceedings of the 5th Int. Particle Accelerator Conf.* **IPAC2014**, 5 pages, 0.551 MB (2014). URL http://jacow.org/ipac2014/doi/JACoW-IPAC2014-MOXBA01.html. Artwork Size: 5 pages, 0.551 MB ISBN: 9783954501328 Medium: PDF Publisher: JACoW Publishing, Geneva, Switzerland.

[4] Simoulin, V. The synchrotron generations. *Revue francaise de sociologie* **57**, 503–528 (2016). URL https://www.cairn-int.info/article-E_RFS_573_0503--the-synchrotron-generations.htm. Bibliographie_available: 1 Cairndomain: www.cairn-int.info Cite Par_available: 1 Publisher: Presses de Sciences Po.

[5] Liu, L. & Jr, H. W. Towards Diffraction Limited Storage Ring Based Light Sources (2017).

[6] Liu, L., Neuenschwander, R. T. & Rodrigues, A. R. D. Synchrotron radiation sources in Brazil. *Philosophical Transactions of the Royal Society A* (2019). URL https://royalsocietypublishing.org/doi/10.1098/rsta.2018.0235. Publisher: The Royal Society Publishing.

[7] Liu, L. *et al.* Status of Sirius Operation. *Proceedings of the 13th International Particle Accelerator Conference* **IPAC2022**, 4 pages, 0.882 MB (2022). URL https://jacow.org/ipac2022/doi/JACoW-IPAC2022-TUPOMS002.html. Artwork Size: 4 pages, 0.882 MB ISBN: 9783954502271 Medium: PDF Publisher: JACoW Publishing, Geneva, Switzerland.

[8] Liu, L., Oliveira, A. & Tavares, D. Status of SIRIUS operation with users (2022).

[9] Liu, L., Resende, X. R. & Rodrigues, A. R. D. Injection Dynamics for Sirius Using a Nonlinear Kicker 3 (2016).

[10] de Sá, F. H., Liu, L. & Resende, X. R. Optimization of Nonlinear Dynamics for Sirius (2016).

[11] Dester, P. S., Sá, F. H. & Liu, L. Energy acceptance and on momentum aperture optimization for the Sirius project. *Journal of Physics: Conference Series* **874**, 012068 (2017). URL https://doi.org/10.1088/1742-6596/874/1/012068. Publisher: IOP Publishing.

APPENDIX A

Proof of the necessary condition for vectors conjugacy

Lorem ipsum dolor sit amet, consectetuer adipiscing elit. Ut purus elit, vestibulum ut, placerat ac, adipiscing vitae, felis. Curabitur dictum gravida mauris. Nam arcu libero, nonummy eget, consectetuer id, vulputate a, magna. Donec vehicula augue eu neque. Pellentesque habitant morbi tristique senectus et netus et malesuada fames ac turpis egestas. Mauris ut leo. Cras viverra metus rhoncus sem. Nulla et lectus vestibulum urna fringilla ultrices. Phasellus eu tellus sit amet tortor gravida placerat. Integer sapien est, iaculis in, pretium quis, viverra ac, nunc. Praesent eget sem vel leo ultrices bibendum. Aenean faucibus. Morbi dolor nulla, malesuada eu, pulvinar at, mollis ac, nulla. Curabitur auctor semper nulla. Donec varius orci eget risus. Duis nibh mi, congue eu, accumsan eleifend, sagittis quis, diam. Duis eget orci sit amet orci dignissim rutrum.

Nam dui ligula, fringilla a, euismod sodales, sollicitudin vel, wisi. Morbi auctor lorem non justo. Nam lacus libero, pretium at, lobortis vitae, ultricies et, tellus. Donec aliquet, tortor sed accumsan bibendum, erat ligula aliquet magna, vitae ornare odio metus a mi. Morbi ac orci et nisl hendrerit mollis. Suspendisse ut massa. Cras nec ante. Pellentesque a nulla. Cum sociis natoque penatibus et magnis dis parturient montes, nascetur ridiculus mus. Aliquam tincidunt urna. Nulla ullamcorper vestibulum turpis. Pellentesque cursus luctus mauris.

Nulla malesuada porttitor diam. Donec felis erat, congue non, volutpat at, tincidunt tristique, libero. Vivamus viverra fermentum felis. Donec nonummy pellentesque ante. Phasellus adipiscing semper elit. Proin fermentum massa ac quam. Sed diam turpis, molestie vitae, placerat a, molestie nec, leo. Maecenas lacinia. Nam ipsum ligula, eleifend at, accumsan nec, suscipit a, ipsum. Morbi blandit ligula feugiat magna. Nunc eleifend consequat lorem. Sed lacinia nulla vitae enim. Pellentesque tincidunt purus vel magna. Integer non enim. Praesent euismod nunc eu purus. Donec bibendum quam in tellus. Nullam cursus pulvinar lectus. Donec et mi. Nam vulputate metus eu enim. Vestibulum pellentesque felis eu massa.

Quisque ullamcorper placerat ipsum. Cras nibh. Morbi vel justo vitae lacus tincidunt ultrices. Lorem ipsum dolor sit amet, consectetuer adipiscing elit. In hac

habitasse platea dictumst. Integer tempus convallis augue. Etiam facilisis. Nunc elementum fermentum wisi. Aenean placerat. Ut imperdiet, enim sed gravida sollicitudin, felis odio placerat quam, ac pulvinar elit purus eget enim. Nunc vitae tortor. Proin tempus nibh sit amet nisl. Vivamus quis tortor vitae risus porta vehicula.

Fusce mauris. Vestibulum luctus nibh at lectus. Sed bibendum, nulla a faucibus semper, leo velit ultricies tellus, ac venenatis arcu wisi vel nisl. Vestibulum diam. Aliquam pellentesque, augue quis sagittis posuere, turpis lacus congue quam, in hendrerit risus eros eget felis. Maecenas eget erat in sapien mattis porttitor. Vestibulum porttitor. Nulla facilisi. Sed a turpis eu lacus commodo facilisis. Morbi fringilla, wisi in dignissim interdum, justo lectus sagittis dui, et vehicula libero dui cursus dui. Mauris tempor ligula sed lacus. Duis cursus enim ut augue. Cras ac magna. Cras nulla. Nulla egestas. Curabitur a leo. Quisque egestas wisi eget nunc. Nam feugiat lacus vel est. Curabitur consectetuer.

Suspendisse vel felis. Ut lorem lorem, interdum eu, tincidunt sit amet, laoreet vitae, arcu. Aenean faucibus pede eu ante. Praesent enim elit, rutrum at, molestie non, nonummy vel, nisl. Ut lectus eros, malesuada sit amet, fermentum eu, sodales cursus, magna. Donec eu purus. Quisque vehicula, urna sed ultricies auctor, pede lorem egestas dui, et convallis elit erat sed nulla. Donec luctus. Curabitur et nunc. Aliquam dolor odio, commodo pretium, ultricies non, pharetra in, velit. Integer arcu est, nonummy in, fermentum faucibus, egestas vel, odio.

Sed commodo posuere pede. Mauris ut est. Ut quis purus. Sed ac odio. Sed vehicula hendrerit sem. Duis non odio. Morbi ut dui. Sed accumsan risus eget odio. In hac habitasse platea dictumst. Pellentesque non elit. Fusce sed justo eu urna porta tincidunt. Mauris felis odio, sollicitudin sed, volutpat a, ornare ac, erat. Morbi quis dolor. Donec pellentesque, erat ac sagittis semper, nunc dui lobortis purus, quis congue purus metus ultricies tellus. Proin et quam. Class aptent taciti sociosqu ad litora torquent per conubia nostra, per inceptos hymenaeos. Praesent sapien turpis, fermentum vel, eleifend faucibus, vehicula eu, lacus.

Pellentesque habitant morbi tristique senectus et netus et malesuada fames ac turpis egestas. Donec odio elit, dictum in, hendrerit sit amet, egestas sed, leo. Praesent feugiat sapien aliquet odio. Integer vitae justo. Aliquam vestibulum fringilla lorem. Sed neque lectus, consectetuer at, consectetuer sed, eleifend ac, lectus. Nulla facilisi. Pellentesque eget lectus. Proin eu metus. Sed porttitor. In hac habitasse platea dictumst. Suspendisse eu lectus. Ut mi mi, lacinia sit amet, placerat et, mollis vitae, dui. Sed ante tellus, tristique ut, iaculis eu, malesuada ac, dui. Mauris nibh leo, facilisis non, adipiscing quis, ultrices a, dui.

Morbi luctus, wisi viverra faucibus pretium, nibh est placerat odio, nec commodo wisi enim eget quam. Quisque libero justo, consectetuer a, feugiat vitae, porttitor eu, libero. Suspendisse sed mauris vitae elit sollicitudin malesuada. Maecenas ultricies eros sit amet ante. Ut venenatis velit. Maecenas sed mi eget dui varius euismod. Phasellus

aliquet volutpat odio. Vestibulum ante ipsum primis in faucibus orci luctus et ultrices posuere cubilia Curae; Pellentesque sit amet pede ac sem eleifend consectetuer. Nullam elementum, urna vel imperdiet sodales, elit ipsum pharetra ligula, ac pretium ante justo a nulla. Curabitur tristique arcu eu metus. Vestibulum lectus. Proin mauris. Proin eu nunc eu urna hendrerit faucibus. Aliquam auctor, pede consequat laoreet varius, eros tellus scelerisque quam, pellentesque hendrerit ipsum dolor sed augue. Nulla nec lacus.

Suspendisse vitae elit. Aliquam arcu neque, ornare in, ullamcorper quis, commodo eu, libero. Fusce sagittis erat at erat tristique mollis. Maecenas sapien libero, molestie et, lobortis in, sodales eget, dui. Morbi ultrices rutrum lorem. Nam elementum ullamcorper leo. Morbi dui. Aliquam sagittis. Nunc placerat. Pellentesque tristique sodales est. Maecenas imperdiet lacinia velit. Cras non urna. Morbi eros pede, suscipit ac, varius vel, egestas non, eros. Praesent malesuada, diam id pretium elementum, eros sem dictum tortor, vel consectetuer odio sem sed wisi.

Appendix B

Algorithms Pseudocode

Lorem ipsum dolor sit amet, consectetuer adipiscing elit. Ut purus elit, vestibulum ut, placerat ac, adipiscing vitae, felis. Curabitur dictum gravida mauris. Nam arcu libero, nonummy eget, consectetuer id, vulputate a, magna. Donec vehicula augue eu neque. Pellentesque habitant morbi tristique senectus et netus et malesuada fames ac turpis egestas. Mauris ut leo. Cras viverra metus rhoncus sem. Nulla et lectus vestibulum urna fringilla ultrices. Phasellus eu tellus sit amet tortor gravida placerat. Integer sapien est, iaculis in, pretium quis, viverra ac, nunc. Praesent eget sem vel leo ultrices bibendum. Aenean faucibus. Morbi dolor nulla, malesuada eu, pulvinar at, mollis ac, nulla. Curabitur auctor semper nulla. Donec varius orci eget risus. Duis nibh mi, congue eu, accumsan eleifend, sagittis quis, diam. Duis eget orci sit amet orci dignissim rutrum.

Nam dui ligula, fringilla a, euismod sodales, sollicitudin vel, wisi. Morbi auctor lorem non justo. Nam lacus libero, pretium at, lobortis vitae, ultricies et, tellus. Donec aliquet, tortor sed accumsan bibendum, erat ligula aliquet magna, vitae ornare odio metus a mi. Morbi ac orci et nisl hendrerit mollis. Suspendisse ut massa. Cras nec ante. Pellentesque a nulla. Cum sociis natoque penatibus et magnis dis parturient montes, nascetur ridiculus mus. Aliquam tincidunt urna. Nulla ullamcorper vestibulum turpis. Pellentesque cursus luctus mauris.

Nulla malesuada porttitor diam. Donec felis erat, congue non, volutpat at, tincidunt tristique, libero. Vivamus viverra fermentum felis. Donec nonummy pellentesque ante. Phasellus adipiscing semper elit. Proin fermentum massa ac quam. Sed diam turpis, molestie vitae, placerat a, molestie nec, leo. Maecenas lacinia. Nam ipsum ligula, eleifend at, accumsan nec, suscipit a, ipsum. Morbi blandit ligula feugiat magna. Nunc eleifend consequat lorem. Sed lacinia nulla vitae enim. Pellentesque tincidunt purus vel magna. Integer non enim. Praesent euismod nunc eu purus. Donec bibendum quam in tellus. Nullam cursus pulvinar lectus. Donec et mi. Nam vulputate metus eu enim. Vestibulum pellentesque felis eu massa.

Quisque ullamcorper placerat ipsum. Cras nibh. Morbi vel justo vitae lacus tincidunt ultrices. Lorem ipsum dolor sit amet, consectetuer adipiscing elit. In hac habitasse platea dictumst. Integer tempus convallis augue. Etiam facilisis. Nunc elementum fermentum wisi. Aenean placerat. Ut imperdiet, enim sed gravida sollicitudin, felis odio

placerat quam, ac pulvinar elit purus eget enim. Nunc vitae tortor. Proin tempus nibh sit amet nisl. Vivamus quis tortor vitae risus porta vehicula.

Fusce mauris. Vestibulum luctus nibh at lectus. Sed bibendum, nulla a faucibus semper, leo velit ultricies tellus, ac venenatis arcu wisi vel nisl. Vestibulum diam. Aliquam pellentesque, augue quis sagittis posuere, turpis lacus congue quam, in hendrerit risus eros eget felis. Maecenas eget erat in sapien mattis porttitor. Vestibulum porttitor. Nulla facilisi. Sed a turpis eu lacus commodo facilisis. Morbi fringilla, wisi in dignissim interdum, justo lectus sagittis dui, et vehicula libero dui cursus dui. Mauris tempor ligula sed lacus. Duis cursus enim ut augue. Cras ac magna. Cras nulla. Nulla egestas. Curabitur a leo. Quisque egestas wisi eget nunc. Nam feugiat lacus vel est. Curabitur consectetuer.

Suspendisse vel felis. Ut lorem lorem, interdum eu, tincidunt sit amet, laoreet vitae, arcu. Aenean faucibus pede eu ante. Praesent enim elit, rutrum at, molestie non, nonummy vel, nisl. Ut lectus eros, malesuada sit amet, fermentum eu, sodales cursus, magna. Donec eu purus. Quisque vehicula, urna sed ultricies auctor, pede lorem egestas dui, et convallis elit erat sed nulla. Donec luctus. Curabitur et nunc. Aliquam dolor odio, commodo pretium, ultricies non, pharetra in, velit. Integer arcu est, nonummy in, fermentum faucibus, egestas vel, odio.

Sed commodo posuere pede. Mauris ut est. Ut quis purus. Sed ac odio. Sed vehicula hendrerit sem. Duis non odio. Morbi ut dui. Sed accumsan risus eget odio. In hac habitasse platea dictumst. Pellentesque non elit. Fusce sed justo eu urna porta tincidunt. Mauris felis odio, sollicitudin sed, volutpat a, ornare ac, erat. Morbi quis dolor. Donec pellentesque, erat ac sagittis semper, nunc dui lobortis purus, quis congue purus metus ultricies tellus. Proin et quam. Class aptent taciti sociosqu ad litora torquent per conubia nostra, per inceptos hymenaeos. Praesent sapien turpis, fermentum vel, eleifend faucibus, vehicula eu, lacus.

Pellentesque habitant morbi tristique senectus et netus et malesuada fames ac turpis egestas. Donec odio elit, dictum in, hendrerit sit amet, egestas sed, leo. Praesent feugiat sapien aliquet odio. Integer vitae justo. Aliquam vestibulum fringilla lorem. Sed neque lectus, consectetuer at, consectetuer sed, eleifend ac, lectus. Nulla facilisi. Pellentesque eget lectus. Proin eu metus. Sed porttitor. In hac habitasse platea dictumst. Suspendisse eu lectus. Ut mi mi, lacinia sit amet, placerat et, mollis vitae, dui. Sed ante tellus, tristique ut, iaculis eu, malesuada ac, dui. Mauris nibh leo, facilisis non, adipiscing quis, ultrices a, dui.

Morbi luctus, wisi viverra faucibus pretium, nibh est placerat odio, nec commodo wisi enim eget quam. Quisque libero justo, consectetuer a, feugiat vitae, porttitor eu, libero. Suspendisse sed mauris vitae elit sollicitudin malesuada. Maecenas ultricies eros sit amet ante. Ut venenatis velit. Maecenas sed mi eget dui varius euismod. Phasellus aliquet volutpat odio. Vestibulum ante ipsum primis in faucibus orci luctus et ultrices posuere cubilia Curae; Pellentesque sit amet pede ac sem eleifend consectetuer. Nullam

elementum, urna vel imperdiet sodales, elit ipsum pharetra ligula, ac pretium ante justo a nulla. Curabitur tristique arcu eu metus. Vestibulum lectus. Proin mauris. Proin eu nunc eu urna hendrerit faucibus. Aliquam auctor, pede consequat laoreet varius, eros tellus scelerisque quam, pellentesque hendrerit ipsum dolor sed augue. Nulla nec lacus.

Suspendisse vitae elit. Aliquam arcu neque, ornare in, ullamcorper quis, commodo eu, libero. Fusce sagittis erat at erat tristique mollis. Maecenas sapien libero, molestie et, lobortis in, sodales eget, dui. Morbi ultrices rutrum lorem. Nam elementum ullamcorper leo. Morbi dui. Aliquam sagittis. Nunc placerat. Pellentesque tristique sodales est. Maecenas imperdiet lacinia velit. Cras non urna. Morbi eros pede, suscipit ac, varius vel, egestas non, eros. Praesent malesuada, diam id pretium elementum, eros sem dictum tortor, vel consectetuer odio sem sed wisi.